Masterarbeit in Physik
angefertigt im
Helmholtz - Institut für Strahlen- und Kernphysik

Dynamic quadrupole interaction in semiconductor

vorgelegt der
Mathematisch-Naturwissenschaftlichen Fakultät
der
Rheinischen Friedrich-Wilhelms-Universität Bonn

von
Dang Thien Thanh

Bonn, September 2013

Anfertigung mit der Genehmigung
der Mathematisch-Naturwissenschaftlichen Fakultät
der Rheinischen Friedrich-Wilhelms-Universität Bonn

Gutachter: ***Privatdozent Dr. Reiner Vianden***

Gutachter(in): ***Prof. Dr. Karl Maier***

I hereby declare that this thesis was formulated by myself and that no sources or tools other than those cited were used.

Bonn, …… .....

Contents

1. Introduction

In recent years, semiconductors like Germanium (Ge), Silicon (Si), Gallium Arsenide (GaAs), and Indium Phosphide (InP) have vast applications in many fields, especially in electronics and optics. Ge and Si are elemental semiconductors with small indirect band gap, whereas InP and GaAs are compound group III-V semiconductors with large direct band gap. Therefore, Ge and Si are very poor at light emission. However, many recent advances make Si possible for light emitting diodes (LEDs) and laser. Besides, Germania (GeO_2) is utilized in optical fibers because of its high index of diffraction and low optical dispersion. With the large band gap, GaAs and InP can emit light efficiently and they can be used in laser diodes. Moreover, they are also used in electronics such as manufacturing high power, high frequency electronics, microwave, solar cell, … Nowadays, GaAs and InP doped Mn or Fe are diluted magnetic semiconductors, and play important role in spintronics. Regarding to Silicon, it has also been widely used in electronics. Si has extremely stable structure and very fine thermal conductor, so it has been chosen in manufacturing integrated circuit (ICs) and nanoelectronics. In addition, the most advantage of Si is that its high holes mobility enables it to be used in high speed *p* channel field effect transistors, needed for CMOS logic. Germanium also has important contribution in electronics. Ge-Si alloys play an essential role in high speed integrated circuits. Ge and GaAs have quite similar lattice constant, and therefore Ge can be also used in solar cell. The enormous contributions of such semiconductors in technology are the motivation for me to study their nanostructures by using perturbed angular correlation technique.

The perturbed angular correlation (PAC) technique has been applied to study the nanostructure of solids in general and semiconductors in specific in recent several decades. Thanks to the PAC spectroscopy one can clearly understand about crystalline structure and electronic structure at an atomic scale. The theory of PAC will be presented in the following sections. In my thesis, the PAC technique has been carried out by implanting radioactive source ^{111}In, which decays into the ground state of ^{111}Cd via two successive gamma rays emission, into semiconductors like Ge, Si, InP and GaAs. The observation of the impact of external fields like electric or magnetic field on the correlation between the emitted directions of the two gamma rays has given us information about the microscopic crystal environment of the probe ^{111}In.

The external fields can be the electric field gradient (EFG), resulting from the change distribution of the host lattice after ion implantation process or from the “aftereffects” caused by electron capture decay of ^{111}In. The interaction between this EFG and the electric quadrupole moment *Q* of the intermediate state of the probe nucleus is called electric quadrupole interaction (EQI). Besides EFG, the extra field can be created by externally applying the magnetic field with the magnitude of 0.48 T and 2.1 T. The interaction between such magnetic fields with the nuclear magnetic dipole moment of the intermediate state of the probe nucleus is called magnetic dipole interaction (MDI).

Both EQI and NDI can cause the perturbation on angular correlation of two gamma rays emitted from the decay of ^{111}In. Thanks to the PAC theory we can measure the transition frequencies of sublevels in the intermediate state by using the theoretical functions to fit the experimental spectra. The frequency magnitudes provide us much understanding about structure of the host lattice surrounding the probe ^{111}In.

My measurements consist of three parts: measuring at low temperatures (from 12 K to 110 K) annealed samples (Si, Ge, GaAs, InP) to study dynamic quadrupole interaction (part 1); measuring the annealed samples in magnetic field with magnitudes of 0.48 T and 2.1 T to observe magnetic interaction (part 2); measuring the annealed sample in magnetic field of 0.48 T and in liquid nitrogen (77 K) simultaneously to evaluate the combination of electric interaction and magnetic interaction (part 3). The first part is major study of my thesis. In the second part, I only use the PAC method to measure the Larmor frequency resulting from MDI. The detailed study of the influence of the magnetic field on the angular correlation can be found in the thesis of Ishita Agarwal [AGA12]. In the third part I would only like to show how the Larmor frequency influences on the quadrupole interaction frequency.

The idea of this thesis is to check the results of the experiments studied by A. F. Pasquevich and R. Vianden several decades ago. Nowadays, the quality of the semiconductor material available to us is much better, which may allow us to study purely dynamic interactions because the static damping due to low quality material and intrinsic damage might be separated from the influence of dynamic damping due to the "aftereffects". The study of dynamic interactions using the PAC technique enables us to evaluate the nanostructure of semiconductor material surrounding the probe atom and the influence of the electronic properties of the semiconductor, mainly the band gap. Moreover, the measurements of the temperature dependence of dynamic interaction aimed at the same effect that whether the electron concentration decreases with decreasing temperature and whether this lead to larger damping or not. Finally, we carried out the measurements in magnetic fields because I. Agarwal found some influence of magnetic field on the damping in GaN and AlN [AGA12]. Therefore, it could be possible that the magnetic field influences on the electronic state of the probe atom after the decay to ^{111}Cd.

In this thesis, the evaluation of dynamic interactions is based on the "aftereffects" and the U. Bäverstam and R. Othaz model, which will be presented in more detail in sections 3.4.2 and 3.4.3.

2. Material properties of Germanium (Ge), Silicon (Si), Gallium Arsenide (GaAs), and Indium Phosphide (InP)

2.1. Properties of Silicon (Si) and Germanium (Ge)

2.1.1. Physical properties

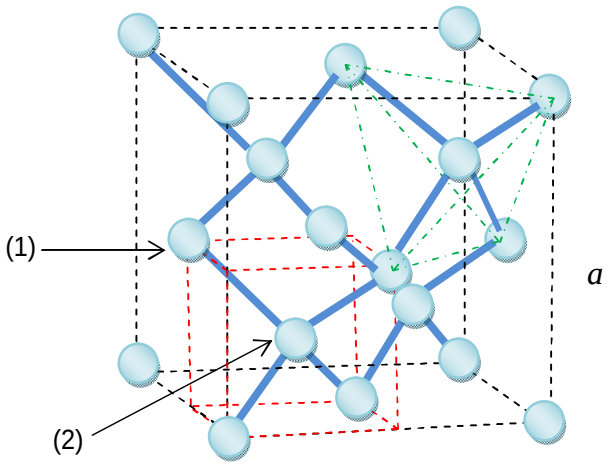

Figure 2.1.1.1. An unit cube for Si and Ge, with a volume a^3 that is four times larger than that of a primitive cell (red lines).

Silicon and Germanium are intrinsic indirect semiconductors and have the same diamond cubic structure consisting of a face centered cubic Bravais point lattice which contains two identical atoms per lattice point. The distance between the two atoms equals one quarter of the body diagonal of the cube. A unit cube for Si and Ge (crystallographic unit cell) is depicted in figure 2.1.1.1. In the unit cube there are 8 corner atoms, 6 face atoms and 4 interior atoms. Each edge of the cube has a length of *a*, which is called lattice constant. In this structure, each atom is surrounded by four equidistant nearest neighbors that stay at the corner of the tetrahedron (the green one in the figure 2.1.1.1). In a primitive cell, there are two kinds of atomic sites: substitutional site and tetrahedral site, where substitutional sites are four corners of the tetrahedron (1) and tetrahedral site locates at the center of the tetrahedron (2). Some important properties of Si and Ge are summarized in table 2.1.1.1.

	Si	Ge
Lattice constant a [Å]	5.43	5.65
Crystal density [g/cm^3]	2.329	5.326
Atomic weight [g/mol]	28.08	72.59
Melting point [$^\circ$C]	1412	937

Table 2.1.1.1. Some important properties of Si and Ge at 300 K, these values are taken from [MOL03].

One interesting property of Si is that a nearly perfect lattice and a very low impurity density (pure element) prevent Si from stoichiometric deviation due to implantation and annealing treatments.

2.1.2. Electrical properties

The electrical properties of Si and Ge depend on temperature and doping with different impurity atoms. Firstly, temperature dependence is one of the most important electrical features. At low temperature range Si and Ge have very low electrical conductivity, and therefore they are nonmetallic material. However, they act like metals at high temperature because of their high electrical conductivity, which can be proved by figure 2.1.2.1. From this we can see that the electrical conductivity of Si exponentially increases with the rising temperature *[MOL03]*.

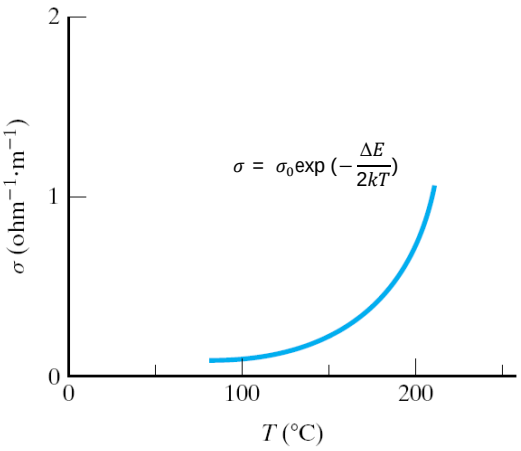

Figure 2.1.2.1. Electrical conductivity of Si versus temperature. This figure is taken from [SHA05].

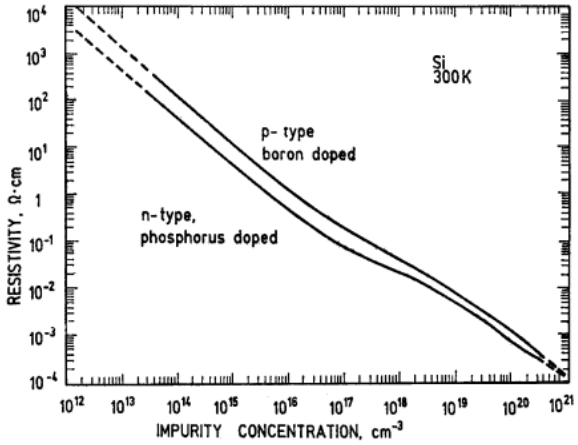

Figure 2.1.2.2. Resistivity versus impurity concentration for Si at 300 K. This figure is taken from [SZE81]

Secondly, the electrical properties of Si and Ge can be changed by doping with different impurity atoms. Silicon and Germanium are intrinsic semiconductors and they become extrinsic semiconductor when doped with impurities. Specifically, they will be a p – type semiconductor if they are doped with group –III acceptor atoms, and they become n – type semiconductor if doped with group – V donor atoms. When Si and Ge are doped with such impurities, their resistivity will be reduced significantly. That is depicted in figure 2.1.2.2 for the case of doping phosphorous and boron. The other essential properties of Si and Ge are summarized in table 2.1.2.1.

	Si	Ge
Energy band gap [eV]	1.12	0.66
Intrinsic carrier concentration [cm^{-3}]	1.45×10^{10}	2.4×10^{13}
Intrinsic resistivity [Ω.m]	2.3×10^{5}	47
Electron mobility (drift) [cm^2/Vs]	1500	3900

Table 2.1.2.1. Some electrical properties of Si and Ge at 300K.

These values are taken from [SAN09] and [SZE81].

2.2. Properties of Gallium Arsenide (GaAs) and Indium Phosphide (InP)

2.2.1. Physical properties

Gallium Arsenide and Indium Phosphide are intrinsic direct semiconductor and have zincblende structure consisting of a face centered cubic Bravais point lattice, depicted in the figure 2.2.1.1. The zincblende structure is essentially the same as diamond structure except for the feature that there are two atom types. The nearest neighbor bond length is one quarter of the body diagonal of the cube, $r_0 = \frac{\sqrt{3}a}{4}$ [BLA82]. In these bonds, Ga and As link to four neighbors As and Ga respectively, similarly for InP. As a result, the a^3 volume-cube contains four GaAs molecules. Other properties of GaAs and InP are summarized in table 2.2.1.1.

	GaAs	InP
Lattice constant *a* [Å]	5.65	5.86
Crystal density [g/cm^3]	5.317	4.79
Atomic weight [g/mol]	144.64	145.8
Melting point [°C]	1238	1060

Table 2.2.1.1. Some important properties of GaAs and InP at 300K.

These values are taken from [BLA82] and [BRI91].

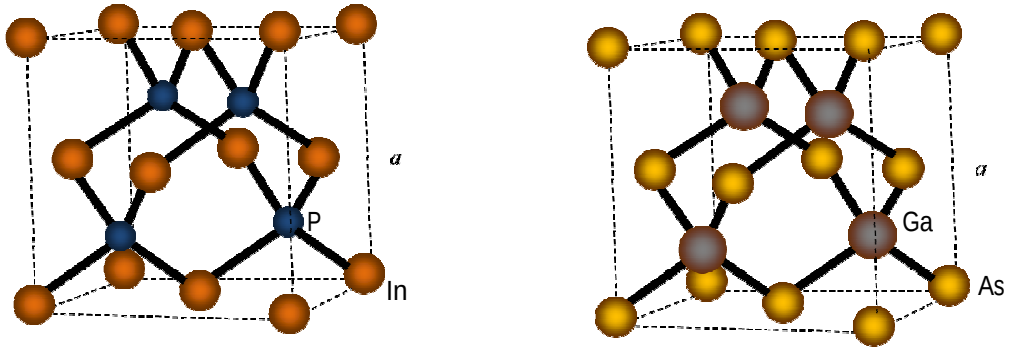

Figure 2.2.1.1. An unit cube for InP(left) and GaAs(right)

2.2.2. Electrical properties

Comparing the values listing in table 2.1.2.1 and 2.2.2.1 we can conclude that some properties of GaAs and InP are superior to those of Si and Ge in some applications. In fact, with higher drift electron mobility, GaAs is used for high-frequency and high-power device. In addition, unlike Si, GaAs has a wider bandgap, allowing it to prevent valence electrons jumping to conduction band, and therefore, GaAs devices are relatively insensitive to heat. The direct band gap also makes it possible for high efficiency of light emission and being used in optoelectronics devices like laser diodes. Due to these advantages, GaAs is widely used in mobile phones, satellite communications, microwave and higher frequency radar systems. The semi-insulating InP has similar electrical properties to GaAs.

	GaAs	InP
Energy band gap [eV]	1.42	1.34
Intrinsic carrier concentration [cm^{-3}]	1.79×10^{6}	1.3×10^{7}
Intrinsic resistivity [Ω.m]	10^{8}	8.6×10^{7}
Electron mobility (drift) [cm^{2}/Vs]	8500	5400

Table 2.2.2.1. Some electrical properties of GaAs and InP at 300K.

These values are taken from [BAR10] and [BRI91].

3. Experimental method

3.1. Theory of angular correlation

The perturbed $\gamma - \gamma$ angular correlation method (PAC) is a popular technique in nuclear condensed matter physics which measures the time dependence of the γ- ray emission pattern. With the PAC technique we can analyze the internal electromagnetic field in solid throughout the hyperfine interaction between the radioactive probe atom and the surrounding fields. Specifically, the electric quadrupole moment Q and magnetic dipole moment $\vec{\mu}$ of the probe atom respectively interact with electric field gradients (EFG) and magnetic field. The EFG is a traceless tensor whose components are the second spatial derivatives of the Coulomb potential $\phi(\vec{r})$ at the nuclear position.

$$V_{ij} = \frac{\partial^2 \phi(\vec{r})}{\partial x_i \, \partial x_j} = \begin{pmatrix} V_{xx} & 0 & 0 \\ 0 & V_{yy} & 0 \\ 0 & 0 & V_{zz} \end{pmatrix}, \tag{3.1.1}$$

where the principal component V_{zz} is the maximum component of the EFG tensor and is generally called the EFG. For cubic lattice, all components of EFG are zero and cannot contribute to electric interactions [SCH92].

In this chapter the discussions about the theory of perturbed $\gamma - \gamma$ angular correlation are based upon the textbook by Schatz and Weidinger [SCH92]. A comprehensive description of this theory can be found in the textbook [FRA65].

As introduced, in this thesis, I focus on analyzing the hyperfine interaction when the probe atom is subjected to an EFG, generally originating from the charge distribution in non-cubic crystal lattice like the wurtztite lattice structure and from non- complete electron shells. With the chosen samples, their lattices have cubic symmetry, so EFG is vanished. Thus the EFG is produced by the non- complete electron shells created by the electron capture “aftereffect”. The “aftereffect” is the electron capture process in decay of ^{111}In. After the ^{111}In captures an electron from the K shell, it becomes ^{111}Cd and leaves a hole in K shell. This hole can move out to the outer shells because of Auger process. The binding of the holes to the probe nuclei causes the fluctuation of the EFG surrounding the probe ^{111}In. The detailed discussion about “aftereffect” will be presented in section 3.4.2. Moreover, the EFG can result from lattice damage due to ion implantation consisting of substitutional and interstitial impurities or vacancies. As introduced, the coupling of EFG at the probe nucleus site to the quadrupole moment Q of the probe nucleus causes electric interaction. The electric interaction can be observed by the time-dependent change of the angular correlation between γ_1 and γ_2 due to an external perturbation.

The electric interaction can be classified into two different interactions: static interaction and time dependent interaction (dynamic interaction).

a) Static interactions result from the interaction between the quadrupole moment Q of the probe atom with static EFG having constant magnitude and direction during the life time of the intermediate state.

b) Dynamic interactions originate from the fluctuating EFG in a liquid environment or in solid due to “aftereffect”.

3.1.1. The unperturbed angular correlation

The aim of this section is to find the angular correlation function of two gamma rays γ_1 and γ_2 emitted from the decay of a radioactive isotope to its ground state. In more detail, a nucleus decays from the initial state $|I_i, M_i>$ to the intermediate state $|I, M>$ by emission of gamma ray γ_1. Then it continuously decays into the final state $|I_f, M_f>$ by emission of gamma ray γ_2. This decay process of a $\gamma - \gamma$ cascade is depicted in figure 3.1.1.1.

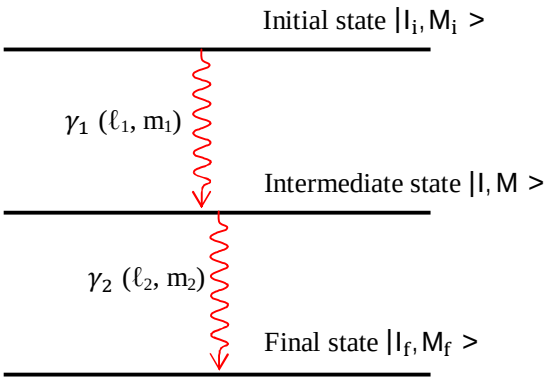

Figure 3.1.1.1. The decay scheme of a $\gamma - \gamma$ cascade.

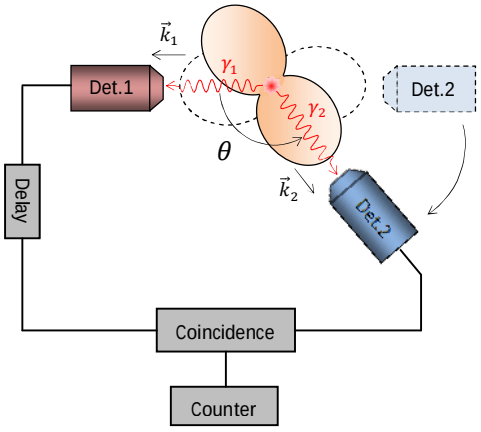

Figure 3.1.1.2. Principle of $\gamma - \gamma$ angular correlation.

Each gamma ray has a defined angular momentum quantum number $l_{1,2}$ and a magnetic quantum number $m_{1,2}$. The transitions must satisfy the following restrictions due to the angular momentum conservation.

$$|\ell_1 - I| \leq I_i \leq |\ell_1 + I| \qquad M_i = m_1 + M \qquad (3.1.1.1)$$

$$|\ell_2 - I_f| \leq I \leq |\ell_2 + I_f| \qquad M = m_2 + M_f \qquad (3.1.1.2)$$

In ordinary circumstances, when considering a large number of nuclei, the directions of the nuclear spins are randomly distributed. Therefore, the probability for the direction of emission is equal for every single gamma ray and the angular distribution is isotropic. In the successive emission of two gamma quanta, the direction of emission

of the second radiation will not be isotropic with respect to the orientation of the nuclear spin and has a certain angular correlation with the first one since the second one is emitted from a state which is populated from the first one, and the angular momentum is conserved. In more detail, in a radioactive source decaying via $\gamma - \gamma$ cascade, an ensemble of nuclei with spins in the same direction is selected. After the first gamma ray is emitted, nuclei in the intermediate state are formed and their magnetic sub-states (m-states) are not equally populated because only some transitions are allowed. To make the selection of the ensemble of nuclei with spins in the same direction, the two gamma rays should be measured in coincidence. The first gamma ray is detected by the fixed detector 1 and the second gamma ray is detected by the movable detector 2 (Figure 3.1.1.2).

The successive emissions of two gamma rays in a nuclear decay are not randomly directed with respect to each other. They obey the so-called angular correlation function. The angular correlation function of two gamma rays is the probability that a nucleus emits γ_1 and γ_2 in direction $\vec{k}_1$ and $\vec{k}_2$ respectively and is denoted by $W(\vec{k}_1, \vec{k}_2)$. The angular correlation function can be written as

$$W(\vec{k}_1, \vec{k}_2) = \sum_{M_i, M_f, \sigma_1, \sigma_2} \left| \sum_M \langle I, M, \vec{k}_1, \sigma_1 | H_1 | I_i, M_i \rangle \langle I_f, M_f, \vec{k}_2, \sigma_2 | H_2 | M \rangle \right|^2 \quad (3.1.1.3)$$

For short notation:

$$W(\vec{k}_1, \vec{k}_2) = \sum_{M_i, M_f, \sigma_1, \sigma_2} |\sum_M \langle M|H_1|M_i\rangle \langle M_f|H_2|M\rangle|^2 \quad (3.1.1.4)$$

H_1, H_2 are the interaction operators for emission of γ_1, γ_2 into direction $\vec{k}_1$, $\vec{k}_2$ with the polarization σ_1 and σ_2 respectively. After calculating the matrix elements we get the equation:

$$W(\vec{k}_1, \vec{k}_2) = W(\theta) = \sum_{k_{even}}^{k_{max}} A_k(1) A_k(2) P_k(\cos\theta) = \sum_{k_{even}}^{k_{max}} A_{kk} P_k(\cos\theta) \quad (3.1.1.5)$$

where *k* is the summation index and obeys the restriction

$$0 \leq k \leq \mathrm{Min}(2I, L_1 + L_1', L_2 + L_2').$$

I is the nuclear spin of the intermediate state. L_1, L_2, L_1', L_2' are multi-polarities of the transitions. Because of parity conservation, *k* is only even. For the probe ^{111}In, *I* = 5/2, L_{12} = 1 or 2 and k_{max} = 4.

$P_k(\cos\theta)$ is the Legendre polynomial in order of θ, which is the angle between $\vec{k}_1$ and $\vec{k}_2$.

The coefficients $A_k(1)$ and $A_k(2)$ depend only on the nuclear spin states and the multi-polarity of the gamma rays. The amplitude of the anisotropic coefficients $A_{kk} = A_k(1).A_k(2)$ are only valid for point-like detectors. For a finite size of the

detector: $A_{kk}^{effective} = A_{kk}.Q_{kk}$, where $Q_{kk} = Q_k(\gamma_1).Q_k(\gamma_2)$ is the so-called damping coefficient.

3.1.2. The perturbed angular correlation

In the case of the unperturbed angular correlation, the interactions of the nucleus with external nuclear fields are not taken into account; therefore, the angular correlation between two gamma rays only depends on the properties of the nuclear decay. When radioactive nuclei are placed in external fields like an electric field and a magnetic field, the hyperfine interaction between the radioactive nuclei with these external fields within the lifetime of the intermediate state will cause the perturbation on the angular correlation (PAC). Then, the angular correlation function in (3.1.1.5) will depend not only on the angle θ but also on the time t. The PAC can be classically explained by the figure 3.1.2.1 where the ^{111}Cd nuclei are placed in a field resulting from two external charges (-q). The hyperfine interaction between the electric quadrupole moment Q of the probe atom with the EFG produced by two charges creates precessions of the nuclei along z-axis. That leads to the changes in the orientation of the nuclear spin and then the changes in the direction of the emission of the second gamma rays. The result of this is the oscillations in the angular correlation of the gamma rays [HEM04].

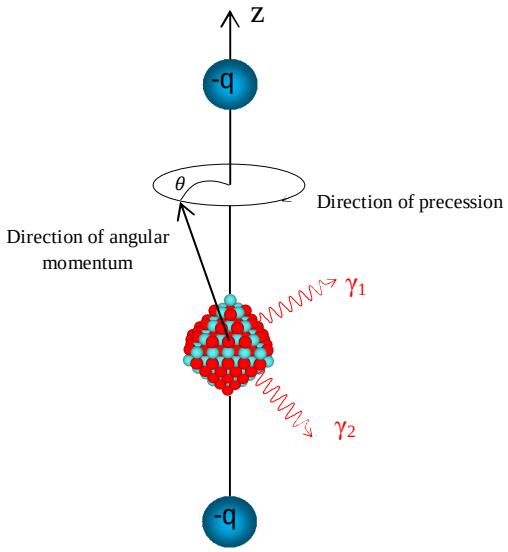

Figure 3.1.2.1. The precession of nuclei in external field caused by two negative charges.

Due to the hyperfine interaction, the intermediate state will be split in to three sub-states shown in figure 3.1.2.2; and therefore, the second gamma ray will then emit from the state $|I, M' >$.

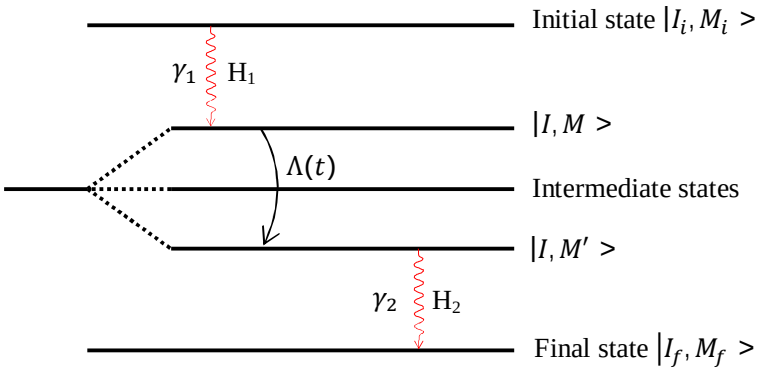

Figure 3.1.2.2. A gamma cascade in the perturbed angular correlation.

In the figure 3.1.2.2, $\Lambda(t)$ is the so-called time evolution operator, causing a transition between the intermediate sublevels. It is quantum mechanically described by a time evolution operator

$$\Lambda(t) = \exp\left(-\frac{i}{\hbar} H_Q t\right), \qquad (3.1.2.1)$$

where H_Q is the interaction operators.

Considering the initially populated sublevel $|M>$, the time evolution operator $\Lambda(t)$ acts on this level can be expressed as

$$|M> \rightarrow \Lambda(t)|M> = \sum_{M'} \langle M'|\Lambda(t)|M\rangle \; |M'> \qquad (3.1.2.2)$$

Therefore, the time-dependent formula for the PAC can be derived from (3.1.1.4) by adding $\Lambda(t)$.

$$W(\vec{k}_1, \vec{k}_2, t) = \sum_{M_i, M_f, \sigma_1, \sigma_2} \left|\sum_M \langle M|H_1|M_i\rangle\langle M_f|H_2\Lambda(t)|M\rangle\right|^2 \qquad (3.1.2.3)$$

After complicated calculations, we get the following formula for time-dependent gamma – gamma angular correlation.

$$W(\vec{k}_1, \vec{k}_2, t) = \sum_{k_1, k_2, N_1, N_2} A_{k_1}(1) A_{k_2}(2)\, G_{k_1 k_2}^{N_1 N_2}(t) \frac{Y_{k_1}^{N_1 *}(\theta_1, \phi_1) Y_{k_2}^{N_2}(\theta_2, \phi_2)}{\sqrt{(2k_1+1)(2k_2+1)}}, \qquad (3.1.2.4)$$

where $G_{k_1 k_2}^{N_1 N_2}(t)$ is the perturbation factor and is defined as

$$G_{k_1 k_2}^{N_1 N_2}(t) = \sum_{M_m, M_m', M_n, M_n'} (-1)^{2I + M_m + M_n} \sqrt{(2k_1+1)(2k_2+1)} \times \begin{pmatrix} I & I & k_1 \\ M_m' & -M_m & N_1 \end{pmatrix}$$

$$\times \begin{pmatrix} I & I & k_2 \\ M_n' & -M_n & N_2 \end{pmatrix} \times \langle M_n|\Lambda(t)|M_m\rangle \langle M_n'|\Lambda(t)|M_m'\rangle^* \qquad (3.1.2.5)$$

Here, the summation index k_{12} are also restricted to $0 \leq k_i \leq \mathrm{Min}(2I, L_1 + L_1', L_2 + L_2')$ like the unperturbed case and $|N_i| \leq k_i$. The $Y_{k_i}^{N_i}$ are spherical harmonics, the angles θ_i and ϕ_i are shown in figure 3.1.2.3.

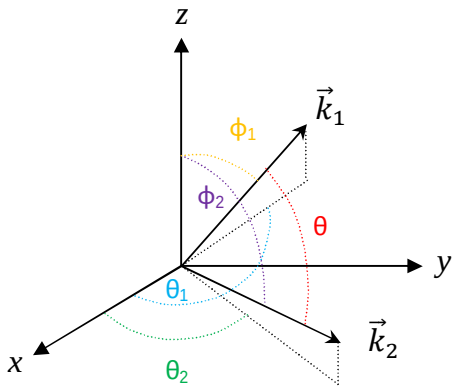

Figure 3.1.2.3. The spatial orientations of γ_1 and γ_2, where γ_1 decays in the direction of $\vec{k}_1$ and γ_2 decays in the direction of $\vec{k}_2$. The angular correlation depends on the angle θ between $\vec{k}_1$ and $\vec{k}_2$.

The perturbation factor in (3.1.2.5) becomes simpler when the interaction is static and the EFG is axial symmetric relative to the z-axis. In this case the time evolution operator is diagonal and presented by

$$\langle M_n|\Lambda(t)|M_m\rangle = \exp\left[-\frac{i}{\hbar}E(M)t\right]\delta_{M,M_m}\delta_{M,M_n} \qquad (3.1.2.6)$$

By inserting Eq. (3.1.2.6) into Eq. (3.1.2.5) we get

$$G_{k_1k_2}^{NN}(t) = \sum_{M,M'} \sqrt{(2k_1+1)(2k_2+1)} \times \begin{pmatrix} I & I & k_1 \\ M' & -M & N \end{pmatrix} \times \begin{pmatrix} I & I & k_2 \\ M' & -M & N \end{pmatrix}$$

$$\times \exp\left[-\frac{i}{\hbar}(E(M) - E(M'))t\right] \qquad (3.1.2.7)$$

Therefore,

$$G_{k_1k_2}(t) \sim \exp\left[-\frac{i}{\hbar}\left(E(M) - E\left(M'\right)\right)t\right] \sim \exp(-i\omega t) \qquad (3.1.2.8)$$

This is the perturbation function, leading to the time-dependent oscillation of the angular correlation.

In the Eq (3.1.2.8) ω is the transition frequency between the m-substates. For electric quadrupole interactions, the transition frequency ω is a result of the interaction between the local electric field gradient (EFG) and the quadrupole moment of the probe nucleus. The EFG was defined in the expression (3.1.1). In order to measure the symmetry of the EFG with respect to quantization axis z (the principal axis system) we use the quantity called asymmetric parameter η.

$$\eta = \frac{V_{xx} - V_{yy}}{V_{zz}}, \qquad (3.1.2.9)$$

where $|V_{xx}| \leq |V_{yy}| \leq |V_{zz}|$ and $0 \leq \eta \leq 1$.

The electric field gradient tensor can be described for most applications by two parameters *i.e.* V_{zz} and η. However, we often use the quadrupole coupling constant $\nu_Q$instead of V_{zz}. The value $\eta = 0$ corresponds to the case of axially symmetric field. In this case, the interaction energy E_M can be determined by formula (3.1.2.10).

$$E_M = \frac{3M^2 - I(I+1)}{4I(2I-1)} eQV_{zz} \qquad (3.1.2.10)$$

Here, I is nuclear spin of the intermediate state. For ^{111}In $I = 5/2$. M is the projection of I along the z axis ($M = I$). Q is the quadrupole moment of the nucleus (in the intermediate state) subjected to the external field. For ^{111}In, $Q(5/2^+) = 0.83(13)$b [SCH92].

The energy difference between two sub-states M and M' is calculated as follows:

$$\Delta E = E_M - E_{M'} = \frac{3eQV_{zz}}{4I(2I-1)} |M^2 - M'^2| \qquad (3.1.2.11)$$

Here $\omega_Q = \frac{eQV_{zz}}{4I(2I-1)\hbar} = \frac{2\pi}{4I(2I-1)}\nu_Q$ where $\nu_Q = \frac{eQV_{zz}}{h}$ is the so-called electric quadrupole interaction frequency.

Therefore,

$$\Delta E = E_M - E_{M'} = 3\hbar\omega_Q |M^2 - M'^2| \qquad (3.1.2.12)$$

The quantity $|M^2 - M'^2|$ is always an integer since $(M^2 - M'^2) = (M + M')(M - M')$. Therefore, all transition frequencies are integer multiples of the smallest non-vanishing transition frequency ω_0, where $\omega_0 = 6\omega_Q$ for half integer nuclear spin I and $\omega_0 = 3\omega_Q$ for integer nuclear spin I. For example, for I = 5/2,

$$\omega_0 = 6\omega_Q = \frac{6eQV_{zz}}{4I(2I-1)\hbar} = \frac{3\pi}{10}\nu_Q \qquad (3.1.2.13)$$

From (3.1.2.12), it is clearly seen that the energy difference depends on the nuclear spin $\vec{I}$, so the splitting is not equidistant as shown in the Fig. 3.1.2.4.

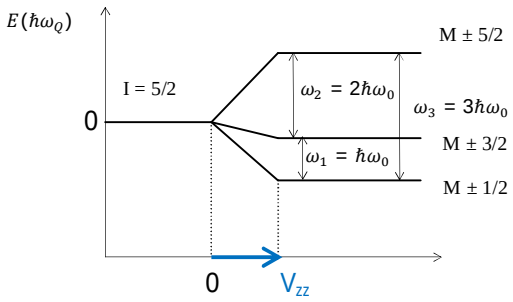

Figure 3.1.2.4. The energy splitting of the I = 5/2 nuclear level for η=0.

The figure 3.1.2.4 is an example of energy splitting of the nuclear spin I = 5/2 for η = 0, where the ratio of the transition frequencies is $\omega_1 : \omega_2 : \omega_3$ = 1:2:3. The lowest transition frequency in this case is $\omega_1 = \omega_0$, the remaining frequencies can be obtained by the relation $\omega_n = n\omega_0$(n = 1, 2, 3). For example ^{111}In with spin I = 5/2, the transition frequencies are:

$$\omega_1 = 1\omega_0 = 6\omega_Q$$

$$\omega_2 = 2\omega_0 = 12\omega_Q$$

$$\omega_3 = 3\omega_0 = 18\omega_Q$$

The perturbation function in (3.1.2.7) can be written more clearly as

$$G_{k_1k_2}^{NN}(t) = \sum_n s_{nN}^{k_1k_2} \cos(n\omega_0 t) \qquad (3.1.2.14)$$

with $s_{nN}^{k_1k_2} = \sum_{M,M'} \sqrt{(2k_1+1)(2k_2+1)} \times \begin{pmatrix} I & I & k_1 \\ M' & -M & N \end{pmatrix} \times \begin{pmatrix} I & I & k_2 \\ M' & -M & N \end{pmatrix}$

In the case of axially symmetric (η = 0) quadrupole interaction, the perturbation factor $G_{kk}(t)$ is independent of N = M – M', and $k_1 = k_2 = k$ [FRA65]. Since A_4 is near zero, only k = 2 is used. For the nuclear spin I = 5/2, the perturbation factor in (3.1.2.14) becomes:

$$G_{22}(t) = s_{20} + \sum_{n=1}^{3} s_{2n} \cos(n\omega_0 t) \exp(-n\delta\omega_0 t) \qquad (3.1.2.15)$$

In the Eq. (3.1.2.15), a static damping δ should be taken into account if the EFG varies slightly at different probe atoms leading to a Gaussian shaped distribution around a mean value [DEI93]. The exponential function accounts for a Lorentzian frequency distribution of relative width δ (static damping) around ω_n.

After being implanted into semiconductors, the probe atoms can be located in different environments of the host lattice, so they are not exposed to uniform interaction. Each type of environment shows distinct EFGs and causes a distinct perturbation. We assume that f_i is the fraction of the probe atoms located in the environment i (i = 1,2, …). The f_i must satisfy $\sum_i f_i = 1$. With this assumption the perturbation factor in (3.1.2.15) becomes:

$$G_{22}(t) = \sum_i f_i \left(s_{20,i} + \sum_{n=1}^{3} s_{2n,i} \cos(n\omega_{0,i} t) \exp(-n\delta_i \omega_{0,i} t)\right) \qquad (3.1.2.16)$$

From this equation we can conclude that $G_{22}(t)$ is a superposition of cosine functions of transition frequencies and s_{2n} are the normalized amplitude for each transition frequency. The perturbation contains all information about the interaction and it depends on the asymmetry parameter η, the angle between $\vec{k}_1$ and $\vec{k}_2$, the orientation of the EFG, and the position of detectors relative to the crystal lattice.

3.2. PAC probe (^{111}In)

In PAC measurements, the used radioactive probe atom must decay via a gamma-gamma cascade. The important requirements for these nuclei are that they have to satisfy some criteria such as a long mean life time of the intermediate state, large electric quadrupole moment and anisotropic coefficient (A_{kk}). In more detail, the mean life time of the intermediate state should be long enough, in the range between 10 ns to several µs to enhance the probability of detecting the second gamma ray from the same nucleus, and short enough to reduce the noise signal. In addition, the electric quadrupole moment Q should be higher than 0.1 barn to make sure that the time-dependence angular correlation can be observed in the PAC window [SCH92]. The half life time of the parent isotope must be sufficiently long so that the sample is still strong after some measurements.

The isotope ^{111}In is an ideal probe for all measurements in this thesis since it meets all the criteria listed above. The decay scheme of ^{111}In is presented in figure 3.2.1.

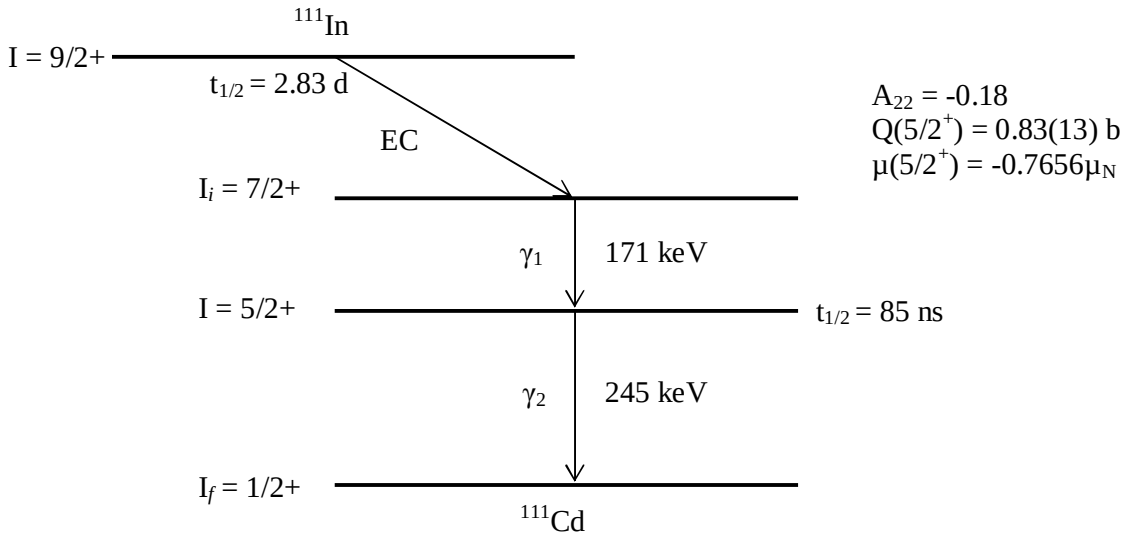

Figure 3.2.1. Decay scheme of 111In

The parent nucleus (^{111}In) decays to an excited state of ^{111}Cd with a nuclear spin of I_i = 7/2+ via electron capture process. This is followed by the decays of the nucleus to ground state of ^{111}Cd by emitting of two successive gamma rays. Specifically, from the state of spin I_i = 7/2+ the nucleus decays to the intermediate state of spin I = 5/2+ by emitting of first gamma ray with the energy of 171 keV. After the time of $t_{1/2}$ = 85 ns, the nucleus will decay to the ground state of spin I_f = ½ by emitting second gamma ray with energy 245 keV. The value for anisotropic coefficient (A_{kk}), electric quadrupole moment Q and magnetic dipole moment μ are shown in the figure 3.2.1.

3.3. Experimental setup

The successive emissions of two gamma rays from ^{111}In decays are detected in coincidence by two out of four detectors A, B, C, D oriented as the figure 3.3.1. The coincidence of the first gamma (start signal) and the second gamma (stop signal) from the two detectors are shown in the table below the figure 3.3.1, where the two opposite detectors create four coincident spectra, and eight coincident spectra come from four pairs of neighboring detectors. The four detectors are stably placed in such a way that the two neighboring detectors are perpendicular. These four detectors use Lutetium Oxyorthosilicate ($Lu_2SiO_5:Ce^{3+}$ or LSO) as scintillation material. The coincident count rate is measured by means of LSO circuit depicted as follows:

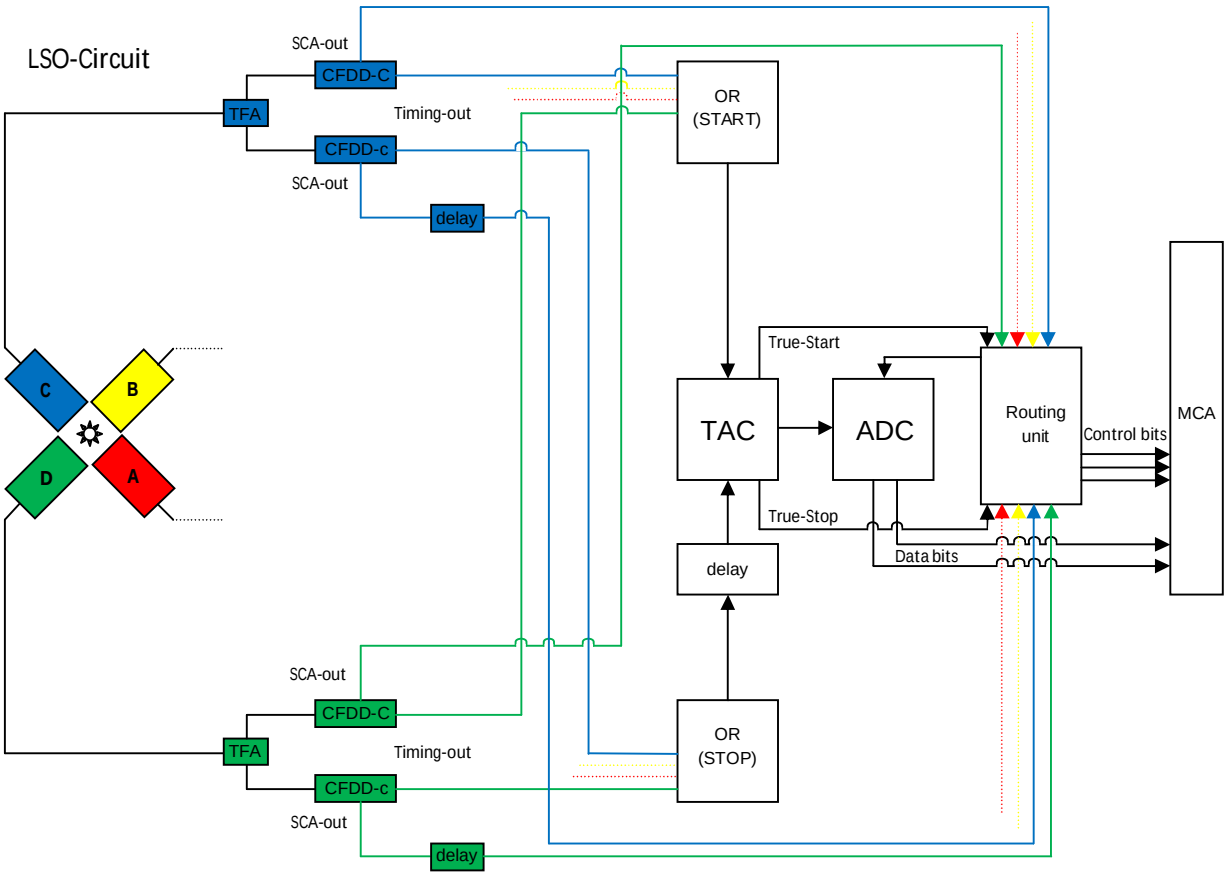

	1	2	3	4	5	6	7	8	9	10	11	12
Start	A	C	A	D	B	C	B	D	A	B	C	D
Stop	c	a	d	a	c	b	d	b	b	a	d	c

Figure 3.3.1. A schematic view of LSO circuit. For simplicity, only the electronic circuits for two detectors are depicted.

From the circuit we can see that each detector only has one output for the time and energy signal. In each output, there are two fast constant fraction differential discriminators (CFDD), containing SCA for start and stop signal. The SCA filters those gamma rays having proper energies for the gamma-gamma cascade. The time measurements are processed by time to amplitude converter (TAC). The TAC is used in order to convert the time different between two digital input signals into analog output signal. After that the output analog signal is digitized by Analog-to-Digital Converters (ADC) and stored in Multichannel-Analyzer (MCA). As mentioned above, we can obtain twelve coincident spectra for start and stop signal which must be separated. This can be done by the routing unit.

3.4. Data analysis

3.4.1. Calculation of anisotropy value R(t)

As described in previous section 3.3, in the experiment four detectors are placed at an angle of 90° relative to each other. For time measurement, each detector can detect the first gamma ray (start signal) and the second gamma ray (stop signal) emitted from different nuclei in the radioactive source. If one out of four detectors receives the start signal, one of the remaining three detectors may detect the stop signal. Therefore, in total we have 12 coincidence spectra in which 8 spectra come from two detectors at

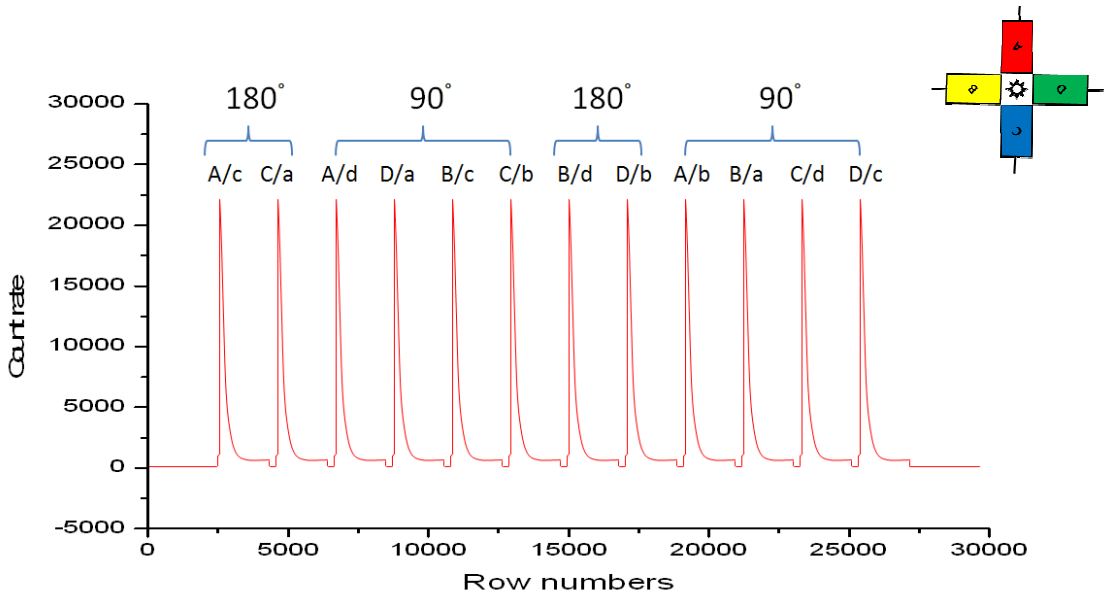

Figure 3.4.1.1 The 12 coincidence spectra $N_i(\theta,t)$ were accumulated simultaneously at the angles $\theta = 90^\circ$ and $\theta = 180^\circ$ between the detectors.

90° and 4 spectra come from two detectors at 180° (Fig. 3.4.1.1).

The count rate of a single coincidence spectrum of two detectors depends on the angle θ between start and stop signal and the time *t*.

$$N_{ij}(\theta,t) = N_0 \epsilon_i \epsilon_j \Omega_i \Omega_j . \exp\left(-\frac{t}{\tau}\right) . W(\theta,t) + U, \qquad (3.4.1.1)$$

where N_0 is the activity of the source at the time zero. ϵ_i and ϵ_j are detector efficiencies. Ω_i and Ω_j are the solid angles covered by the detector. The exponential decay of the intermediate state of gamma-gamma cascade with the life time τ is described by the exponential function $\exp\left(-\frac{t}{\tau}\right)$. The life time curve is modulated by

the angular correlation function $W(\theta, t)$. The record spectra must be corrected by subtracting the background U, which is the random coincidence. This coincidence is caused by the detection of the two gamma rays from different nuclei.

The time dependent ratio function R(t) can be defined as below:

$$R(t) = 2\frac{\bar{N}(180^\circ,t)-\bar{N}(90^\circ,t)}{\bar{N}(180^\circ,t)+2\bar{N}(90^\circ,t)}, \qquad (3.4.1.2)$$

where $\bar{N}(\theta, t)$ is the geometric mean of the background subtracted coincidence count rates.

[SHP02]

$$\overline{N}(180^\circ,t) = \sqrt[4]{\prod_{i=1}^{4} N_i(180^\circ,t)}$$

$$\overline{N}(90^\circ,t) = \sqrt[8]{\prod_{i=1}^{8} N_i(90^\circ,t)}$$

R(t) is also called the anisotropy function since it shows the deviation between the coincidence count rates of a 180° and 90° orientation of two detectors. The calculation of the R(t) is done by the LabVIEW –Program ShowFit. A discussion on various methods for *R*-value formation can be found at [ARE80].

The angular correlation function $W(\theta, t)$ can be expressed as follow:

$$W(\theta, t) \approx 1 + A_{22}.G_{22}(t).P_2(\cos\theta) \qquad (3.4.1.3)$$

In the Eq. (3.4.1.3) the coefficient A_{44} has already neglected since A_{44} is really smaller than A_{22} in the case of probe ^{111}In. $P_2(\cos\theta)$ is called the Legendre polynomials. For simplicity, θ was chosen 90° and 180°, and $P_2(\cos 180^\circ) = 1; P_2(\cos 90^\circ) = -\frac{1}{2}$.

Inserting eq. (3.4.1.3) into eq. (3.4.1.1), and using eq. (3.4.1.2) the relation between the anisotropy R(t) and the perturbation factor $G_{22}(t)$ can be obtained as

$$\mathbf{R(t) = A_{22}G_{22}(t)} \qquad (3.4.1.4)$$

The plots of coincidence count rate between two detectors and the anisotropy (anisotropy spectrum) are presented in figure 3.4.1.2. In the plot of the coincidence count rate (upper), the black curves are the life time curves whereas the modulated life time curve is presented by the red curve. The anisotropy spectrum (lower) is obtained after the exponential decays, detector efficiencies, solid angles and backgrounds are removed, according to the equation (3.4.1.2).

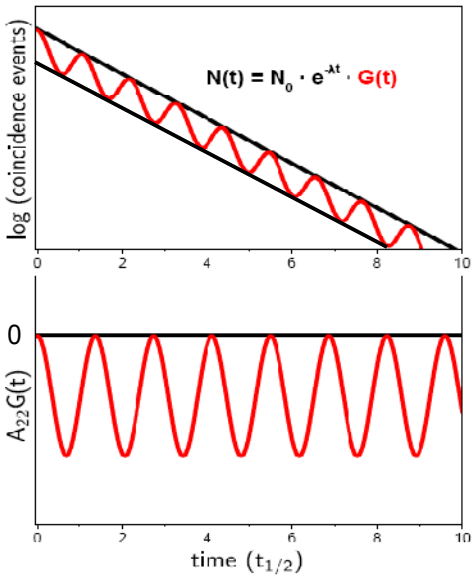

Figure 3.4.1.2. The plots of coincidence count rate (upper) and the anisotropy spectrum (lower) [HAM10].

The anisotropy R(t) contains the desired perturbation factor of the entire information on the interaction and also information about the local electromagnetic fields in the intermediate state [SAN09]. Therefore, all the anisotropy R(t) spectra for dynamic interaction were fitted by the equation (3.4.1.4), using the Nightmare program [NÉD07] based on the NNFit routine [BAR92].

In the equation (3.4.1.4), $G_{22}(t)$ is the static perturbation faction, calculated by the equation (3.1.2.16). After fitting the spectra, the parameters f_i, $\omega_{0,i}$ and δ_i in the equation (3.1.2.16) will be determined. A_{22} is the anisotropic coefficient whose theoretical value is -0.18 for the 172-245 keV gamma ray cascade. This value is only valid for point-like detectors. For the finite size of the detectors the means of anisotropic coefficients were used and they were determined under the help of the Monte Carlo Simulation by the Monte program. The figure 3.4.1.3 will present the plot of the anisotropy coefficients used for the probe ^{111}In as a function of the distance between sample and detector [SAN09].

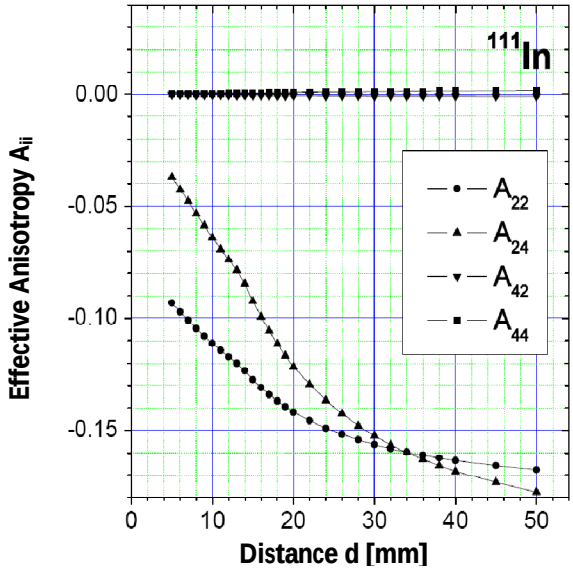

Figure 3.4.1.3. The plot of the simulated anisotropy coefficients [SAN09].

3.4.2. The “aftereffect”

The origin of dynamic interaction in the probe atom site may be ascribed to the so-called “aftereffect” of the electron capture decay of the ^{111}In. The detailed description of “aftereffect” was given by J. E. Thun [THU70]. Here, I would like to give a brief description of the mechanism. The electron capture decay occurs due to the capture of a *K* shell electron by ^{111}In and transforms that isotope into an excited ^{111}Cd nucleus (Figure 3.4.2.1).

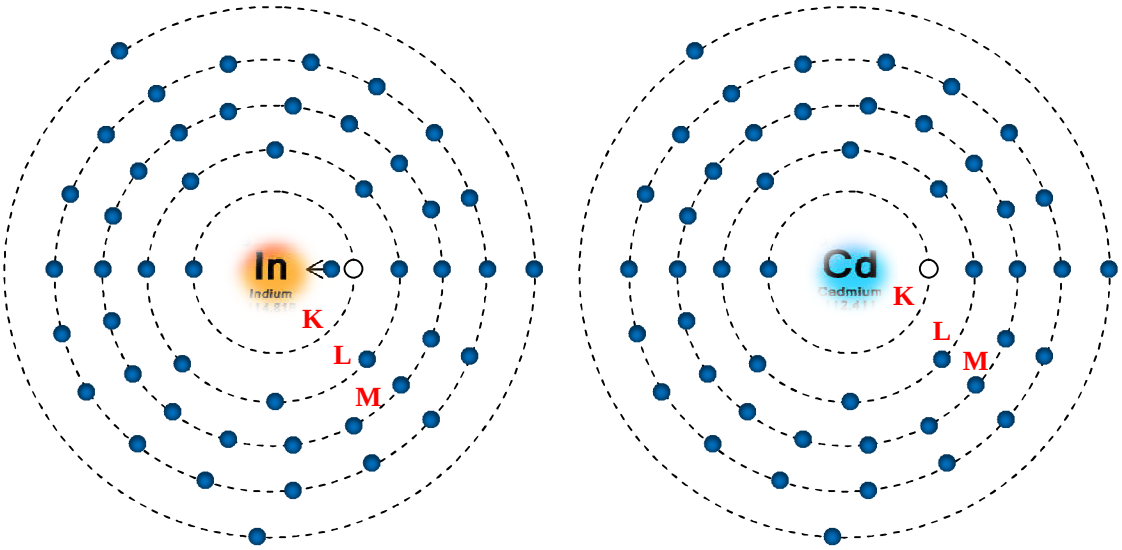

Figure 3.4.2.1. Bohr model of ^{111}In when capturing an electron

After an electron is captured, it leaves an electron vacancy in the inner shells. An electron from a higher energy level may fall into the vacancy, resulting in a release of energy in the form of a photonic emission. This energy can also be transferred to another electron, which is then ejected from the atom. This second ejected electron is called an Auger electron (Figure 3.4.2.2).

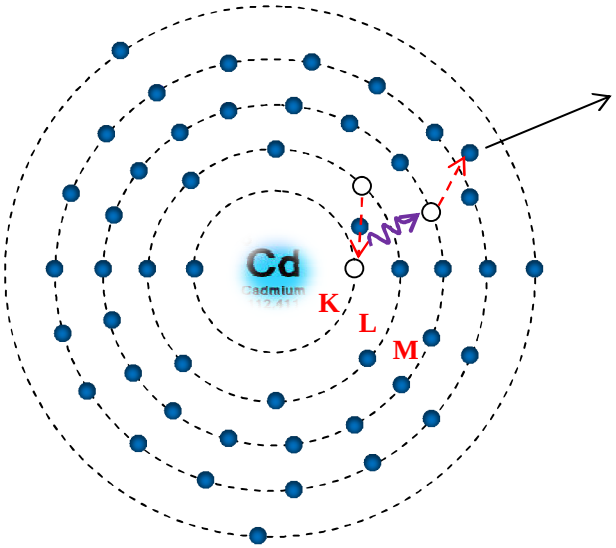

Figure 3.4.2.2: Auger electron

A hole created by *K*- capture will rapidly move out to the outer layers of the atom due to the Auger process. The Auger process is very fast, less than 10^{-12}s, and is independent of the surroundings of the decaying atom [BÄV72]. After a certain time, the number of holes will be multiplied significantly, and the atom may end up in a highly ionized state of the Cadmium. The whole process is the so called "aftereffect". The binding of electron holes at the atomic shell created by Auger process to the probe nuclei causes the fluctuation of the field surrounding the individual probes during the lifetime of the intermediate state of the $\gamma - \gamma$ cascade, leading to the dynamic interaction.

The recovery of the electron shells depends strongly on the electronic surrounding of the probe nucleus [STE10]. When the radioactive atoms are in a metallic environment, these holes will be filled by conduction electrons; and therefore, they have a very short lifetime (in order of ps). This time is so short that the holes cannot cause any perturbation on the directional angular correlation. However, when the atoms are situated in non-metallic materials, the conduction electrons are no longer available [BÄV72]. In this case, the holes might be filled by other ways such as thermionically excited electrons, charge exchange... that allows the holes to remain in appreciable time which is long enough for the hole charge distributions to attenuate the angular correlation.

3.4.3. Evaluation of anisotropy spectra for dynamic interaction. The U. Bäverstam and R. Othaz Model.

For dynamic interaction, U. Bäverstam and R. Othaz [BÄV72] suggested a form for $G_{22}(t)$ basing on the Abragam and Pound [ABR53] theory, from which the R(t) spectra depend on the population of different excited atomic states, the relaxation and recombination of these states. The authors assumed that when the "aftereffects" are involved, the excited atoms, after a certain time, will reach their ground states. At this time, the hyperfine interaction will be static. Two following assumptions will be made:

(i) The probability for an atom to reach its ground state after the time *t* is given by

$$P_g(t) = \lambda_g \exp(-\lambda_g t) = \tau_g^{-1} \exp\left(-\frac{t}{\tau_g}\right), \qquad (3.4.3.1)$$

where λ_g is the atomic recovery constant, and τ_g is the lifetime of dynamic interaction or the time the holes are bound to the probe.

(ii) The mean interaction strength which is characterized by the relaxation constant λ_{2r} remains constant during the dynamic interaction time. The time-dependent contribution to the perturbation factor can be defined as

$$G_{22}^{D}(t) = \left(\frac{\lambda_g}{\lambda_{2r}+\lambda_g}\right) + \frac{\lambda_{2r}}{\lambda_{2r}+\lambda_g}\exp\left(-(\lambda_{2r}+\lambda_g)t\right) \qquad (3.4.3.2)$$

$G_{22}^{D}(t)$ is assumed to be a perturbation factor for purely dynamic interaction. As mentioned, when the excited atoms reach their ground states, the hyperfine interaction will be static. Since this interaction is much weaker than the time –dependent one, the perturbation faction for dynamic interaction $G_{22}(t)$ can be expressed as the product [BÄV72]:

$$G_{22}(t) = G_{22}^{D}(t)G_{22}^{s}(t) \qquad (3.4.3.3)$$

In this formula $G_{22}^{s}(t)$ is perturbation factor for purely static interaction, calculated by (3.1.2.16).

The relaxation constant λ_{2r} and the atomic recovery constant λ_g can be derived from the equation (3.4.3.2) by comparing this equation with the least square fitted function (equation 3.1.2.16). The result shows that the obtained parameters f_i, $\omega_{0,i}$ and δ_i (i = 1, 2) in the equation (3.1.2.16) correspond to those from the equation (3.4.3.2) by the following relations:

$$\begin{cases} \frac{\lambda_g}{\lambda_r+\lambda_g} = f_2 \\ \frac{\lambda_r}{\lambda_r+\lambda_g} = f_1 \\ \lambda_r + \lambda_g = \delta_1\omega_{0,1} \end{cases} \Leftrightarrow \begin{cases} \lambda_g = f_2\delta_1\omega_{0,1} \\ \lambda_r = f_1\delta_1\omega_{0,1} \end{cases} \qquad (3.4.3.4)$$

Here, the fraction f_2 is the fraction of atoms participating in static interaction and called static fraction. The parameters f_1 is the fraction of atoms participating in dynamic interaction and called dynamic fraction. The frequency $\omega_{0,1}$ and the damping δ_1 belong to dynamic interaction.

4. Sample preparation

4.1. Ion implantation

The semiconductors studied in my thesis are pure Si, InP, GaAs and p-type Ge (doped with 10^{10}Boron/cm^3).All samples were implanted with ^{111}In. The probe implantations were done at the Bonn Radioisotope Separator and Implanter, HISKP. Before implantation, we must calculate the implantation energy and incident angle of ion beam. The enough implantation energy makes sure that the probe ions are deeply implanted into the semiconductor. The calculation of this energy was done by using the software SRIM (Stopping and Range of Ions in Matter). The implantation energy depends on the masses of the probe ion and atoms in the sample. The suitable incident angle of ion beam is also very important to prevent the probe ions from the channeling effects. Relying on the calculations of former studies in our group, all the implantations in this study were done with an energy of 160 keV at the incident angle of 10°. The implantation fluence is in the order of 10^{12} ions/cm^2.

4.2. Annealing of implantation damage

Ion implantation is a popular method to enter the probe atoms in to solid. However, the disadvantage of this method is to cause damages in the substrate lattice, which can be removed by thermal annealing. All the samples in my study were annealed in vacuum condition in a Rapid Thermal Annealing Apparatus (RTA). The detailed description of RTA can be found in the diploma thesis of Marx [MAR90]. In RTA, the right annealing temperature importantly contributes to the removal of damages. All the samples were annealed in two minutes with the proximity caps, which are correspondingly non-implanted samples, to maintain surface integrity. The annealing temperatures for all samples in this study are summarized the table 4.2.1.

Samples	T(°C)	References
Ge	600	[MOL03]
Si	900	[MOL03]
GaAs	700	[RIS00]
InP	650	[SCH84]

Table 4.2.1. The temperature setting for annealing samples.

4.3. Cryogenic system

The detailed operation principles of cryogenic system were described in the operational manual [TEC78]. In this section I would like to introduce the basic characteristics of the system as well as some important points one needs to know when using this.

The cryogenic system consists of two components: a converted compressor and an expander module where the very low temperatures are generated. In the converted compressor, high purity helium gas is used as the working medium. These two components are connected together by two pipes, one for high-pressure and the other for low-pressure helium.

The helium pressure in the compressor is monitored by the high-pressure and low-pressure gauges. When the compressor at rest, the pressure should be set at around 220psig (1psig = 69mbar). When the system is operating, the pressure is about 300psig at the high-pressure gauge.

The expender module can generate the temperature range between 12K and 300K. First of all, we can cool the system to the minimum temperature (12K) thanks to the high-pressure helium gas provided by the compressor. Then the temperature can be increased by activating a heating resistor located at the end of the second stage cooling part of the expander. The expander has a thermocouple which is mounted at the coldest end of the expander (Fig. 4.3.1). The thermocouple enables us to observe easily the measuring temperature in Kelvin (K) by connecting it with a control unit model. The control unit also provides the temperature control and necessary voltages for the heating resistor.

The important thing is that the setting temperature must be stable during the measurement. Therefore, a good and stable vacuum condition must be created and it must be insulated from the ambient temperature. In order to create vacuum, the vacuum system is installed, and consisting of two main components: rotary pump and diffusion pump. The minimum pressure can be achieved from the vacuum system in the order of 10^{-5} mbar. Besides that, the first and second stage of the expander module can be isolated from the surrounding temperature by using a vacuum shroud. The expander module and the vacuum shroud must be very tight fitted by two O-ring seals in order to maintain the vacuum.

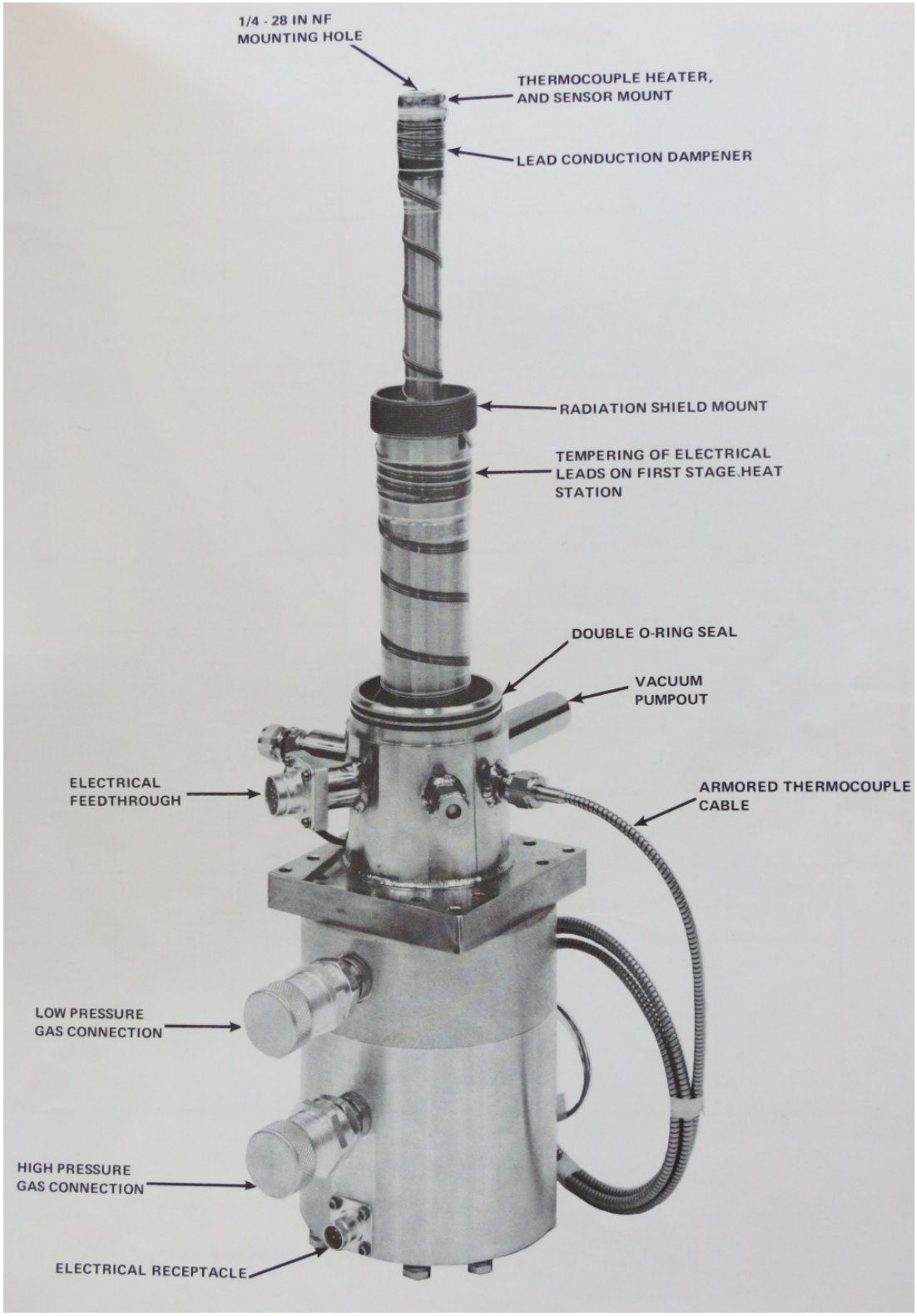

Figure 4.3.1. DE-202 Expander Model with Instrumentation [TEC78]

5. Experimental results and discussions

5.1. Electric quadrupole interaction

As discussed in section 3.1, the electric quadrupole interaction results from the coupling of EFG at the probe nucleus site to the quadrupole moment *Q* of the probe nucleus. The EFG can be found in non-cubic crystal structures or non-complete electron shells. For my studied samples Si, Ge, GaAs, InP, all of them have the cubic crystal. Therefore, the EFG can be created by the non-complete electron shells. In order to observe the dynamic interactions, all the annealed samples were measured at low temperatures since at low temperatures the holes produced by electron capture "aftereffects" can bound to the probe nuclei in appreciable time which is long enough for the hole charge distributions to perturb the angular correlation. The detailed explanation for "aftereffect" is discussed in the section 3.4.2. Before measuring at low temperature the annealed samples, we measured at room temperature (295 K) for as-implanted samples (without thermal annealing) and for annealed samples. For as-implanted samples, the lattices are no longer cubic symmetry because of the damages resulting from ion implantation process, leading to the non-vanishing static EFG. Further information about this will be found in the section 5.1.1.

5.1.1. PAC measurements at room temperature (295 K) for as-implanted samples

Figure 5.1.1.1 depicts anisotropy spectra obtained after measuring as-implanted samples (Ge, Si, InP, and GaAs) without any thermal treatments at room temperature (295 K). All the spectra were fitted by the static perturbation function (3.1.2.16) since the EFG produced by lattice damage has constant magnitude and direction during the life time of the intermediate state, which means that the EFG is purely static.

	f_1(%)	$\omega_{0,1}$(Mrad/s)	ν_{Q1}(MHz)	δ_1(%)	f_2(%)	$\omega_{0,2}$(Mrad/s)	δ_2(%)
Ge	89(2)	190(2)	202(2)	87(5)	10.9(2)	0	0
Si	93(2)	210(14)	223(15)	129(16)	7.3 (2)	0	0
InP	90(3)	156(4)	165(4)	38(2)	9.9(3)	0	0
GaAs	97(5)	187(3)	198(3)	44(1)	3.0(2)	0	0

Table 5.1.1.1. The interaction parameters at room temperature for as implanted samples.

The obtained interaction parameters in table 5.1.1.1 show that the implanted ^{111}In probes were comprised of two fractions f_1 and f_2, which are the fractions of probe atoms involved into the purely static interactions. After implantation (without thermal treatments), only a little amount of the probe atoms (f_2 = 3(2) % to 11(1) %) are situated on lattice sites with nearly cubic symmetry, leading to the vanishing EFG, which is shown by the zero value of interaction frequency for all fraction f_2 in the table

5.1.1.1. These fractions f_2 of probe atoms contribute to the unperturbed angular correlation. The remaining probe atoms (f_1 = 89(2) % to 97(5) %) are located in the non-uniform environment (interstitial impurities), resulting in the perturbations of angular correlation due to electric interaction. The obtained values for f_1 and f_2 are in good agreement with those reported in Mola's PhD thesis [MOL03] for Ge and Si. The obtained static interaction frequencies ν_{Q1}, calculated by the equation (3.1.2.13), are quite large, ranging from 165(4) MHz to 223(15) MHz, and they are widely distributed because of high damping values, varying 38(2) % to 129(16) %. These damping values reflect that the environments surrounding ^{111}In are non-uniform and therefore the EFGs are not homogeneous.

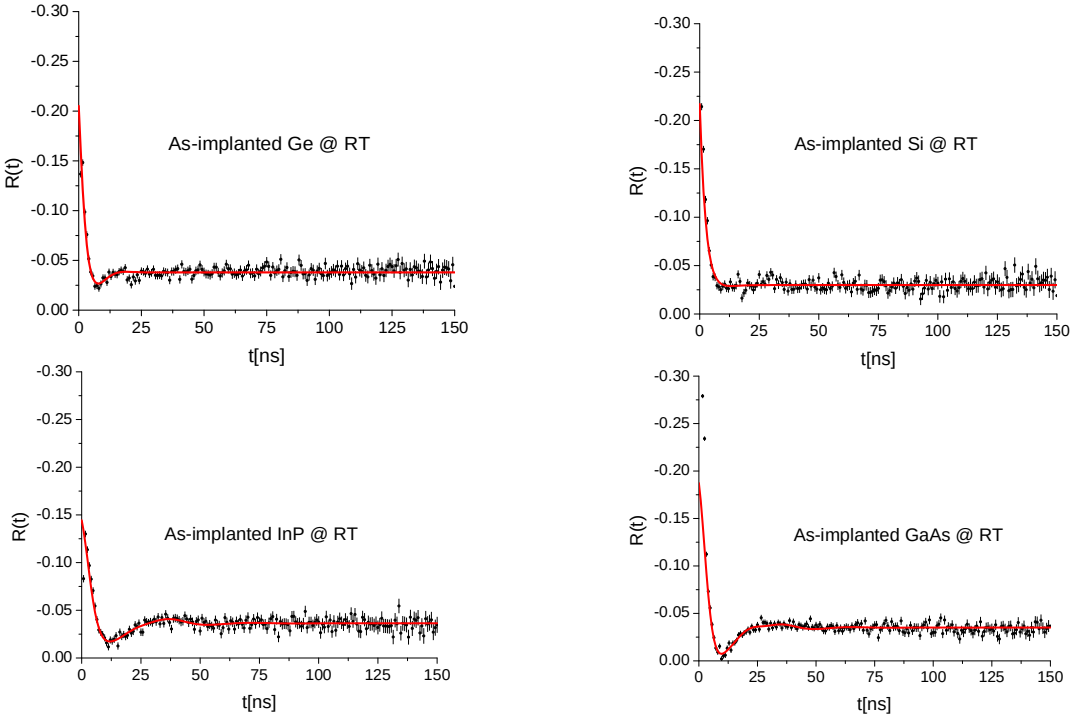

Figure 5.1.1.1. The TDPAC spectra measured at room temperature for as-implanted samples.

The static electric interaction happening inside the studied semiconductors after ^{111}In implantation can result from the lattice point defects, illustrated in the figure 5.1.1.2. In fact, during the implantation process, an energetic probe atom with energy 160 keV penetrates semiconductors and elastically collides with a lattice atom. The result of this collision is the displacement of the lattice atom from the site, leaving behind a vacancy, and the scattering of probe atom in a certain direction. The scattered probe atom might then collide with other lattice atoms. After series of collisions, the probe atom transfers its total energy to lattice atoms and finally stop at some range in the

lattice matrix. If the probe and lattice atom stop at a non-lattice site, they are called interstitials. Both vacancy and interstitials are called point defects. Besides that, there are some other point defects, depicted in figure 5.1.1.2. The point defects can be classified into two categories: intrinsic defects and extrinsic defects [PIC04]. The intrinsic defects consist of only native atoms in the crystal lattice. The extrinsic defects include foreign impurities implanted into the lattice. Specially, after the collision, if the vacancy and the interstitial are created simultaneously, they will be called a Frenkel pair.

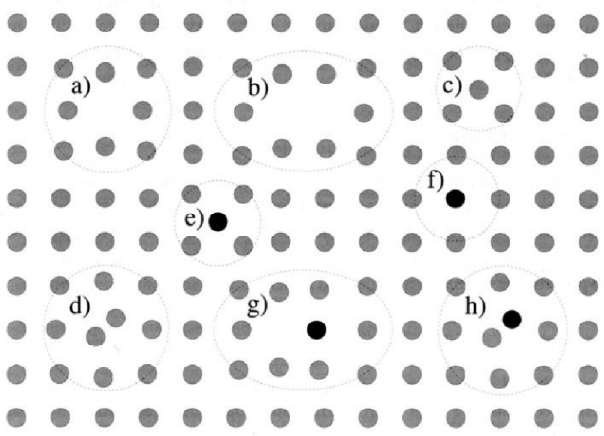

- Intrinsic defects: a, b, c, d

- Extrinsic defects: e, f, g, h

- Specially, *d, g, h,* are named interstitialcy, impurity vacancy pair, impurity self interstitial pair respectively.

Figure 5.1.1.2. Schematic illustration of various defect categories [PIC04]

Due to point defects, the substrate lattices deviate from their cubic symmetries, leading to non-vanishing EFGs.

5.1.2. PAC measurements at room temperature (295 K) for annealed samples

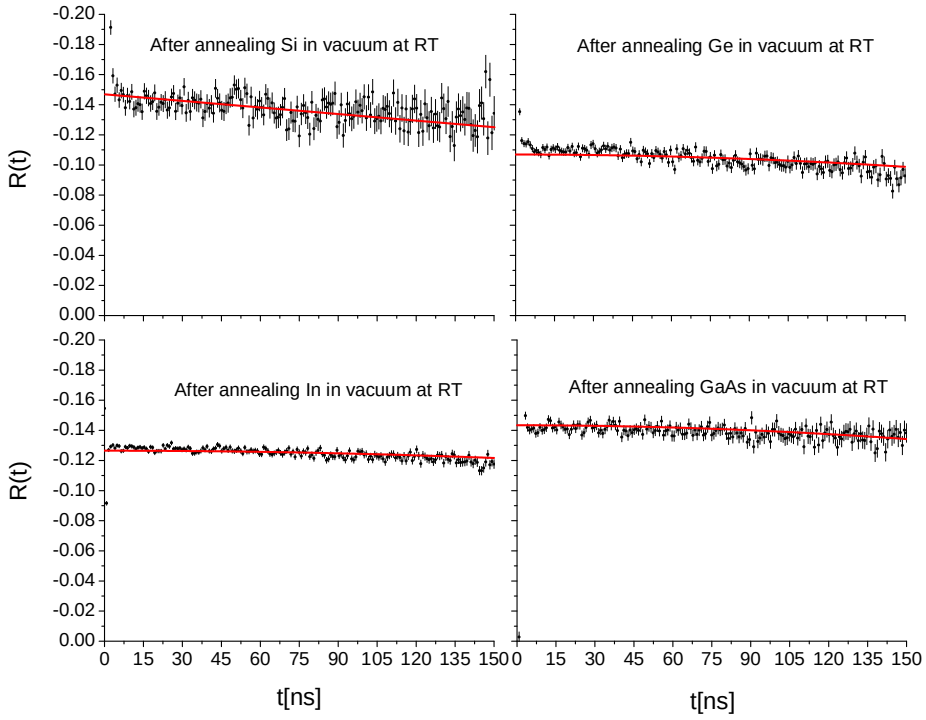

Figure 5.1.2.1. The TDPAC spectra measured at room temperature for annealed samples

All samples were annealed in vacuum by the Rapid Thermal Annealing Apparatus (RTA) with a corresponding cap. The annealing temperatures are shown in table 4.2.1. The TDPAC spectra measured at room temperature (295 K) for annealed samples of Si, Ge, InP, GaAs are shown in figure 5.1.2.1. The fitted parameters for these spectra are shown in table 5.1.2.1, where we can see that after receiving thermal energy, all the probe atoms ($f \approx 100$ %) will replace the host lattice atoms and situate at the sites of cubic symmetry, except for Si. In case of Si, 97(1) % of probe ions locate in the lattice sites. The remaining probe atoms, 3(1) % situate at non-lattice sites experiencing very small EFG ($\nu_{Q2} \approx 0$). In more detail, for Si, the probe atoms will replace Si atoms at the substitutional sites and tetrahedral interstitial sites as well. Although Ge and Si have the same physical properties, the locations of ^{111}In atoms in both lattices are significantly different. The ^{111}In atoms only situate on the substituational sites of the Ge lattice, unlike in the case of Si [MEY70]. For group III – V compound semiconductors like InP and GaAs, it was supposed that ^{111}In will replace the group III atoms in the zinblende structure such as In and Ga [SCH84].

	f_1(%)	ν_{Q1}(MHz)	δ_1(%)	f_2(%)	ν_{Q2}(MHz)	δ_2(%)
Ge	100	1.21(1)	0	0	0	0
Si	97(1)	2.89(9)	0	3(1)	0.0	0
InP	100	0.94(1)	0	0	0	0
GaAs	100	1.37(1)	0	0	0	0

Table 5.1.2.1. The interaction parameter for annealed samples at room temperature

The obtained interaction parameters in the table 5.1.2.1 show that the damages are almost removed by thermal annealing. However, there is an existence of weak static interaction at room temperature in the annealed samples, presented by small values of interaction frequency from 0.94(1) MHz to 2.89(9) MHz. Although almost of the probe atoms populate at the sites of host lattice atoms, the surrounding environments of the probe atoms are not completely cubic symmetry because of the difference in size between the implanted probe atom and lattice atom (Fig.5.1.2.2). In fact, when the probe atom has significant difference in atomic radius with the lattice atom (Table 5.1.2.2), the presence of the probe atom can create the lattice distortion, which can produce small EFG. However, in a cubic lattice, a radially symmetric distortion should cause a cubic distortion and a vanishing EFG at the centre. Therefore, the difference in radius between the probe atom and lattice atom cannot create small EFG. The good explanation for the weakly static interaction could be adsorbate sites on surfaces. After annealing, the probe atoms might situate at or near a surface of the substrates, where the lattice is no longer cubic [SCH92]. This can be the reason leading to the small EFG.

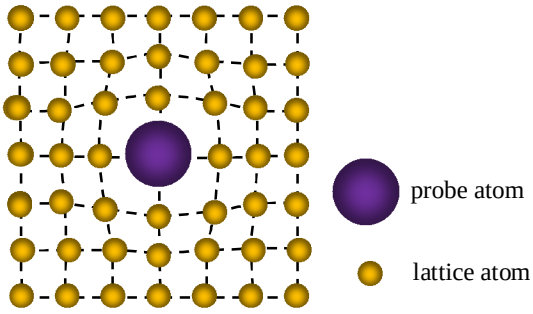

Figure 5.1.2.2. The distortion caused by a substitutional impurity.

	Ge	Si	In	P	Ga	As
Atomic radius [Å]	1.25	1.10	1.55	1.00	1.30	1.15

Table 5.1.2.2. Atomic radii [SLA64].

5.1.3. PAC measurements at low temperature for annealed samples – The experimental results and discussions for dynamic interaction.

After annealing, we carried out the measurements at low temperatures varying from 12 K to 110 K in vacuum. The obtained PAC spectra are fitted by the static function (3.1.2.16) and then evaluated according to the U. Bäverstam formula as presented in section 3.4.3, under the help of the Nightmare program, written by R. Nédélec [NÉD07]. In general, the electric interaction results from the interaction between EFG and the electric quadrupole moment Q of the probe nucleus. In as-implanted samples, the deviations of the lattice from the symmetry, cubic symmetry, for example, produce the static EFG. At room temperature, in the annealed samples, the EFGs vanish because of the recovery of their cubic lattice. However, the appearance of a fluctuating EFGs can be possible at low temperature due to the "after-effect" produced by the electrons capture processes in decay of ^{111}In [BÄV72]. At higher temperature, this effect should still be in the sample but may exist in smaller time scales, so it may not be visible in the PAC measurements. Due to these fluctuating EFGs, the electric interactions become dynamic interactions or time-dependent interactions. According to U. Bäverstam and R. Othaz model, the dynamic interaction can be characterized by relaxation constant λ_r and recovery constant λ_g, which are determined by (3.4.3.4). From this formula, λ_r and λ_g depend on three parameters like fractions, frequency and damping. These three parameters together characterize for dynamic interaction. One parameter cannot individually contribute to dynamic interaction. Therefore, before evaluating dynamic interaction, we should analyze the interaction parameters namely fractions f_i, the frequency ν_Q, damping δ.

A. The experimental results

a. Fractions f_i

The fraction values corresponding to different measured temperatures of each sample are shown in the figure 5.1.3.1, where we can see that the fraction of the probes consists of two parts f_1 and f_2. The fraction f_1 involves dynamic interactions whereas the fraction f_2 shows static interactions. The values for both fractions corresponding to each semiconductor can be found in appendix A. When "aftereffects" are taking place, the fluctuating EFGs, produced by the holes bound to the probe atom, will become static after the time τ_g [PAS87], called lifetime of dynamic interaction. This lifetime will be discussed in section 5.1.3d. Moreover, after the lifetime of the intermediate state $t_{1/2}$ = 85 ns, the excited atoms will reach their ground state and then the interaction will be also static. Therefore, during the observed time of PAC spectrum (x-axis), there are two kinds of fraction: dynamic fraction f_1 and static fraction f_2.

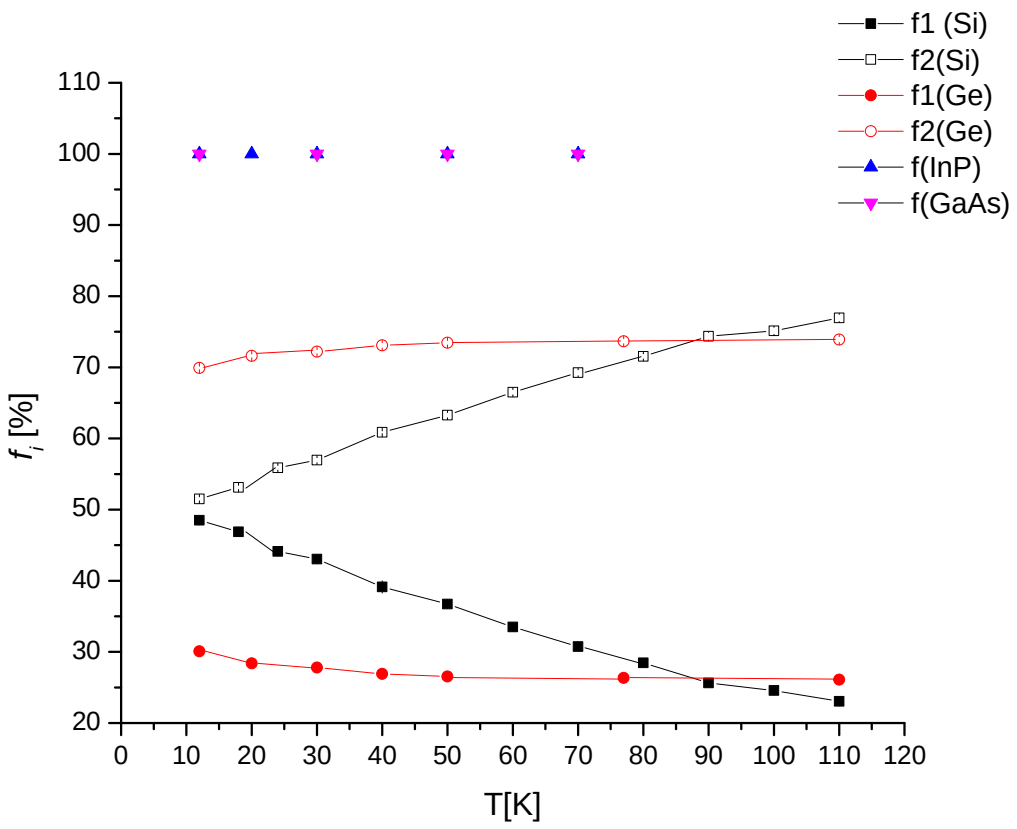

Figure 5.1.3.1. The change of fraction versus temperature.

For Si, the dynamic fraction f_1 decreases gradually versus the rising temperature, whereas the opposite is true for the static fraction f_2. Specifically, the fractions f_1 gradually decline from 48.5(2) % at 12 K to 23.1(1) % at 110 K, while the fractions f_2 gradually grow from 51.5(2) % at 12 K to 76.9(5) % at 110 K. For Ge, the fraction f_1 and f_2 follow the same trend like those in case of Si. However, this is only true for T < 50 K. When the temperature increases from 12 K to 50 K, the fraction f_1 slightly drops from 30.1(1) % to 26.5(1) % whereas the fraction f_2 slightly rises from 69.9(2) % to 73.5(3) %. For T > 50 K, the fraction f_1 and f_2 are stable around 26 % and 74 % respectively. From this we can see that, for Si, the fractions of probe atom change significantly from 12 K to 110 K, whereas they change slightly with measured temperatures for Ge. The increasing fractions f_2 with rising temperature means that the higher the temperature is, the more the number of probe atoms are exposed to static EFG. The explanation for this observation might be due to the increasing number of conduction electrons at high temperature as mentioned in section 2.1.2. These increasing conduction electrons can fill in the holes created by the Auger process in the “aftereffects”, leading to the static EFG surrounded the probe atoms. The number of conduction electron is proportional to the number of filled holes; therefore at higher temperature, the EFG is more static. This explanation, relying on the conduction electrons, can be considered as a model and it is not completely true for all samples,

but in this case it could be a good explanation. For InP and GaAs, the fractions which might be ascribed to the unperturbed fraction are always 100%. In these cases, the dynamic interactions are assumed to be not present. The detailed evaluation for these will be found in next section (5.1.3b).

b. Interaction frequency ν_Q

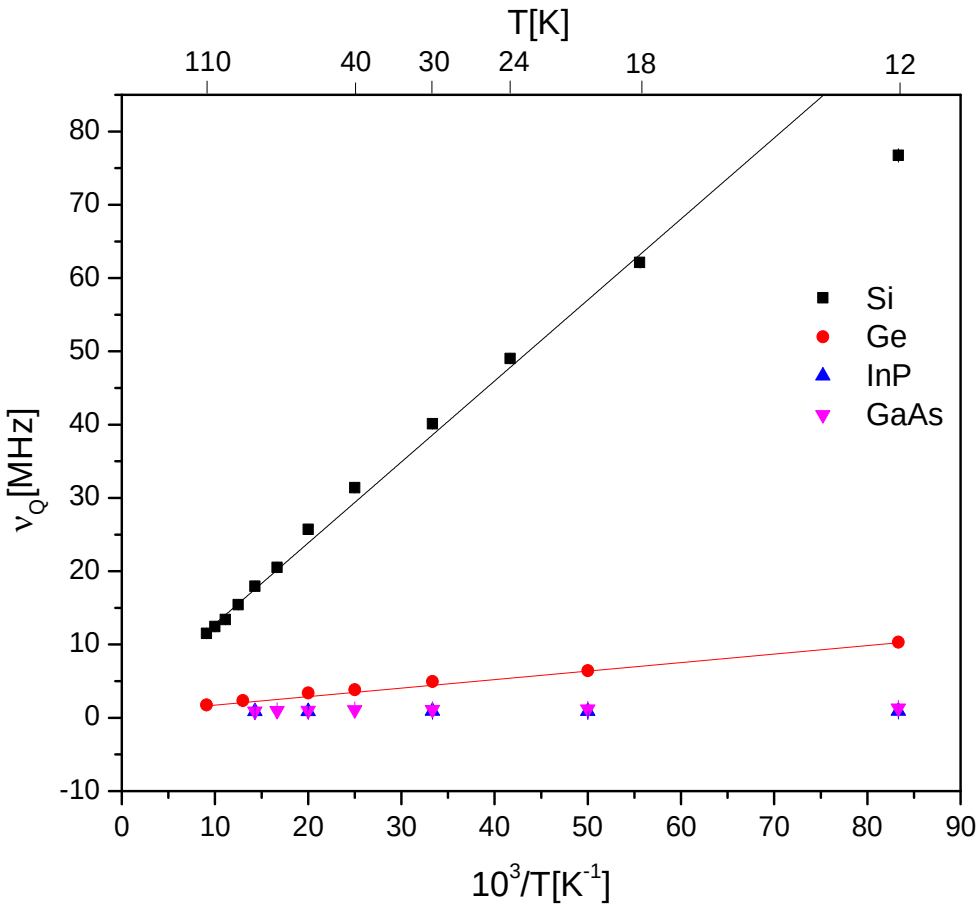

Figure 5.1.3.2. The change of interaction frequency as a function of 1/T

The figure 5.1.3.2 presents the change of interaction frequency ν_Q versus the temperature T for the probe atoms involving in dynamic interactions (fraction f_1). For the probe atoms contributing to static interactions (fraction f_2), the interaction frequency ν_Q is always zero because these probe atoms situate at cubic sites and have complete electron shells, leading to vanishing EFGs. For Ge and Si, the frequency ν_Q linearly increases with 1/T. For InP and GaAs, the frequency ν_Q is very small and independent of the temperature. The illustration for these can be found in figure 5.1.3.2. At the lowest measured temperature 12 K, the frequency is highest at

77(1) MHz and 10.34(6) MHz for Si and Ge respectively. These values decrease gradually, reaching the lowest value 12(1) MHz for Si and 1.75(1) MHz for Ge at the highest measured temperature 110 K. In case of GaAs and InP, the frequencies are very small and stable around 1 MHz for all measured temperatures from 12 K to 70 K. These frequencies are nearly equal to those in the table 5.1.2.1 and may belong to static interactions because the implantation damages might not be completely removed as discussed in section 5.1.2. Moreover, the frequency decreases lightly when the temperature is rising, from 40 K to 110 K, for both Si and Ge. In contrast, when the temperature increases from 12 K to 40 K, the frequency drops sharply. The detailed values for ν_Q at all measured temperatures can be found in the appendix A.

c. Damping δ

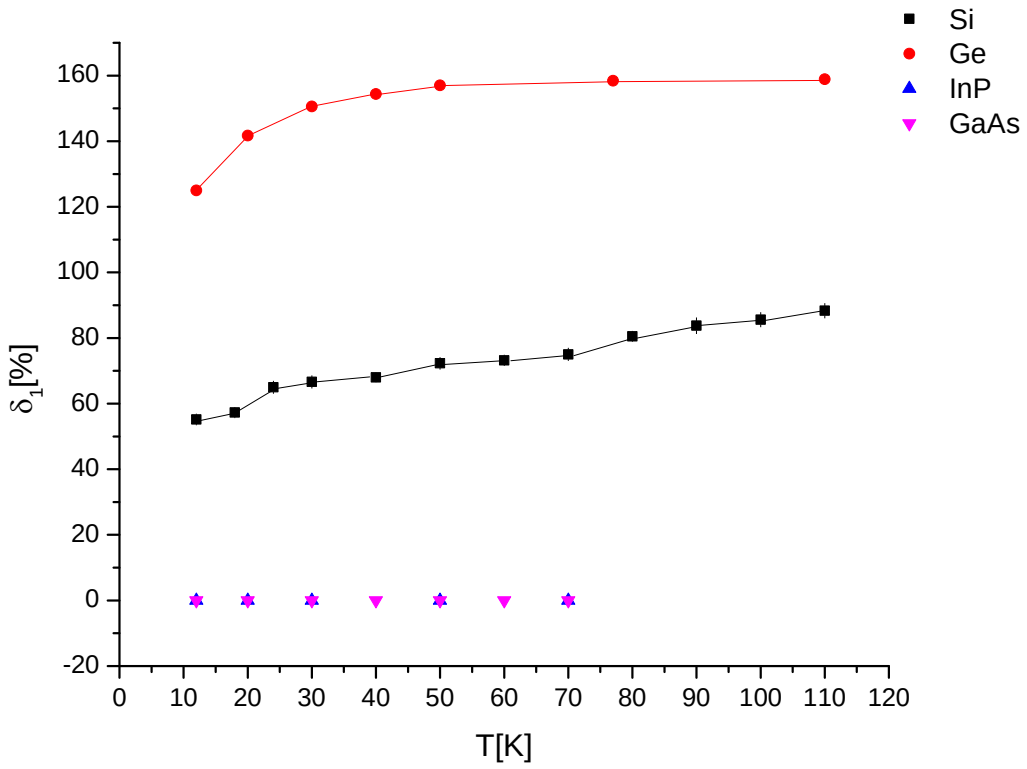

Figure 5.1.3.4. The change of damping versus temperature.

Besides the fractions and interaction frequency, the change of damping versus the temperature depicted in figure 5.1.3.4 also gives us information about dynamic interaction. For Si, with the measured temperature range, the damping generally follows an upward trend when the temperature increases. This is also true for Ge from

12 K to 40 K. In detail, from 12 K to 40 K, the damping values considerably increase from 55(2) % to 68(1) % for Si, and from 125(1) % to 154(2) % for Ge. Above 40 K, while Si continuously follows an upward trend in damping from 68(1) % to 88(2) %, Ge experiences a quite stable damping, around 158(2) %. As shown in the section 3.1.2, the damping represents the homogeneous characteristic of the fields surrounding the probe nuclei. Therefore, the variation of damping in the measured temperatures partly reflects the fluctuation of the EFG produced by the "aftereffect". As discussed in section 5.1.3b, InP and GaAs experience no dynamic interaction, and now the zero damping values also allow us to conclude that the fluctuating EFG does not exist in InP and GaAs lattice.

B. The evaluations and discussions for dynamic interaction

The dynamic interaction can be characterized by relaxation constant λ_r and recovery constant λ_g, according to the U. Bäverstam and R. Othaz model [BÄV72]. The relaxation constant λ_r represents for the strength of dynamic interaction and $\tau_g = \frac{1}{\lambda_g}$ is the life time of the dynamic interaction which means the time the holes are bound to the probe atom. Both parameters λ_r and λ_g are calculated by the equation (3.4.3.4). The values for these two parameters corresponding to each sample are presented in the appendix A.

First, we discuss about the strength of the dynamic interaction. In the case of Si, figure 5.1.3.5 shows that λ_r is always much higher than that in other samples at given temperatures and increases with a second order polynomial function of 1/T. For example, at 12 K λ_r is highest, 19.4(9) MHz. This value decreases gradually, reaching 2.2(1) MHz at 110K. Like Si, the relaxation constant λ_r in the case of Ge also increases with decreasing temperature T. However, in this case λ_r changes as a linear function of 1/T. For instance, the highest value of λ_r at 12 K is lower than that of Si, 3.67(6) MHz. This value becomes smaller at 110 K, 0.68(1) MHz. Moreover, similarly to the interaction frequency ν_Q, the relaxation parameter also declines slowly when the temperature is going up (above 40K) for both Si and Ge. For InP and GaAs, in contrast, this parameter is zero leading to the conclusion that the dynamic interaction cannot happen in InP and GaAs at the measured temperatures, which can be seen by linear fits in appendix B.3 and B.4.

We can conclude that λ_r increases when temperature decreases, which means that the lower the temperature is, the stronger the dynamic interaction becomes for both samples Si and Ge. This property of dynamic interactions might be explained by the "aftereffects". When dynamic interactions take place, the holes need to be bound to the probe. If the picture of Bohr model in the figure 3.4.2.1 is valid, the K shell consists of two electrons which can leave two holes when the electron captures occur. These two

holes are bound to the probe ion and could produce an EFG. At higher temperature, the magnitude of EFG would be lower since the holes may move to excited orbits of larger radius [PAS87], leading to weaker dynamic interactions. However, the measurements at low temperature for InP and GaAs has shown no dynamic interactions. It is explained that for higher average atomic number of the group III-V host, the bonds between the valence electrons and the atomic nucleus are weaker at low temperature [PAS90]. This may be the reason why even at low temperature, the holes can be filled by the conduction electrons, resulting a vanishing EFG.

Moreover, the dynamic interactions in Si are substantially stronger than those in Ge. This property is visibly reflected by spectra in the appendix B.1 and B.2, where the spectra for Ge are less fluctuating than those for Si in first nanoseconds. As discussed in section 5.1.2, after being implanted into Si, the probe atoms can populate on both lattice sites: substitutional sites and tetrahedral interstitial sites (Fig.2.1.1.1), whereas in Ge only the population of the probe atoms on the substitutional sites is found [MEY70]. Therefore, the fluctuating EFG in Si lattice can be produced by the combination of the electron –capture (EC) aftereffects at two different sites, while the EC aftereffects only takes place at one site in Ge lattice. This leads to the magnitude of EFG in Si lattice is much higher than that in Ge, which means that the dynamics interaction in Si is strongest.

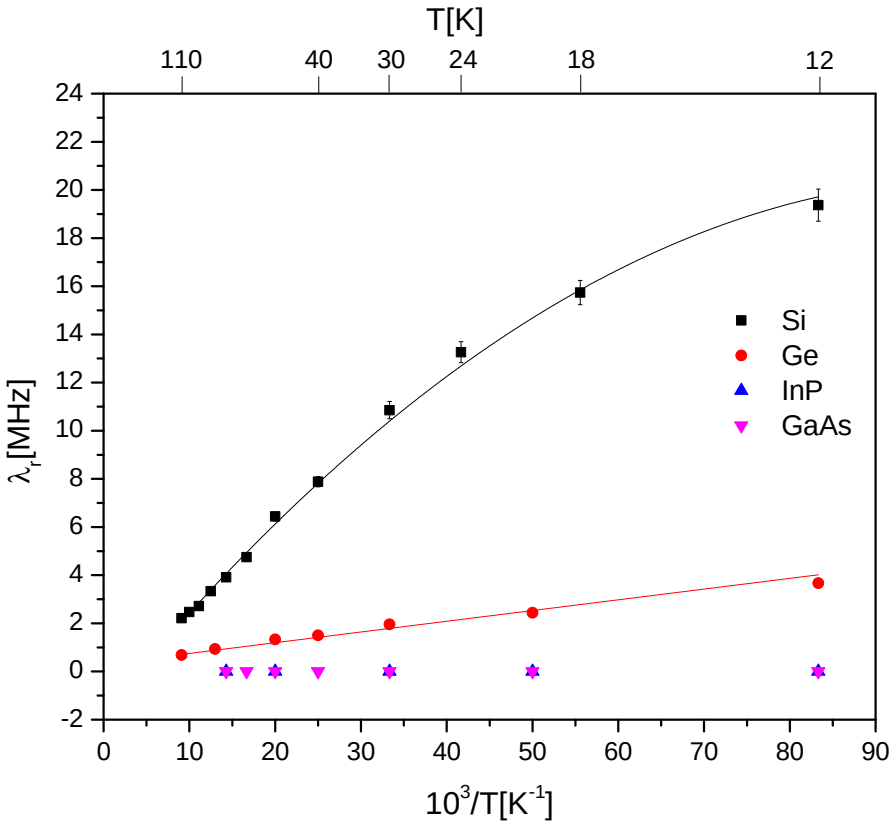

Figure 5.1.3.5. The change of relaxation parameter as a function of temperature

The main difference, i.e. no dynamic interaction in GaAs and InP and stronger dynamic interaction in Si and Ge, is that the former two are direct band gap semiconductors whereas the latter two are indirect band gap semiconductors. In addition, in Si the electron mobility is lowest, which is twice less than that in Ge. In the other two semiconductors, the electron mobility is much larger, which are presented in tables 2.1.2.1 and 2.2.2.1.

As presented in section 2, among four studied semiconductors, Ge has smallest band gap with E_g = 0.66 eV, which is almost twice less than that for Si E_g = 1.12 eV. In contrast, GaAs has largest band gap with E_g = 1.42 eV, followed by InP with E_g = 1.34 eV. In large band gap semiconductor, the number of conduction electron is less than that in small band gap semiconductor; therefore, the number of hole bound to the probe might be higher, leading to a stronger dynamic interaction. This argument contradicts with the obtained results that there are no dynamic interactions in GaAs and InP. Therefore, we could conclude that apparently there are no direct influences of the different band gap and electron concentration on dynamic interaction.

Secondly, the evaluation for the lifetime τ_g of the dynamic interaction is also important. The change of τ_g versus the temperature is shown in figure 5.1.3.6 with the upper one for Si and the lower one for Ge. In general, the lifetime τ_g increases with rising temperature in both samples. For Si, when the temperature increases from 12 K to 110 K, the lifetime τ_g is in the range from 49(2) ns to 135(6) ns. For Ge, the lifetime τ_g is much higher than that in case of Si during the measured temperatures, being in the range from 117(2) ns at 12 K to 516(10) ns at 110 K. When the observed time t > τ_g, the dynamic interaction will switch off and this time interval only shows static interaction. Therefore, during the observed time t of anisotropy spectra (x-axis) of both samples Si and Ge, there is the combination of static and dynamic interactions which well agree with the expression (3.4.3.3) in U. Bäverstam and R. Othaz model.

The increasing of lifetime τ_g with temperature shows that for Si and Ge, the dynamic interaction exists longer at high temperature. As explained in section 5.1.3a that the number of conduction electrons may homogeneously increase in Si and Ge at high temperature. If it is true, at high temperature, the mean distance from the conduction electron to the hole should decrease. We assume that all electrons move with the same constant speed, the time the electrons need to fill the hole created by the “aftereffects” could be shorter. Therefore the holes might be bound to the probe shorter at high T. This argument may contradict with the obtained results for lifetime τ_g. However, the experimental anisotropy spectra in appendix B.1 and B.2 are good agreements with the calculated lifetime τ_g presented in the figure 5.1.3.6 and in appendix A.1 and A.2. The value of lifetime corresponding to each temperature can be marked by dashed line in

each spectrum. Therefore, the using of conduction electron for explaining the increasing of lifetime τ_g with temperature for Si and Ge might not be valid. The explanation for this is still unknown and we will try to find a good explanation in the future.

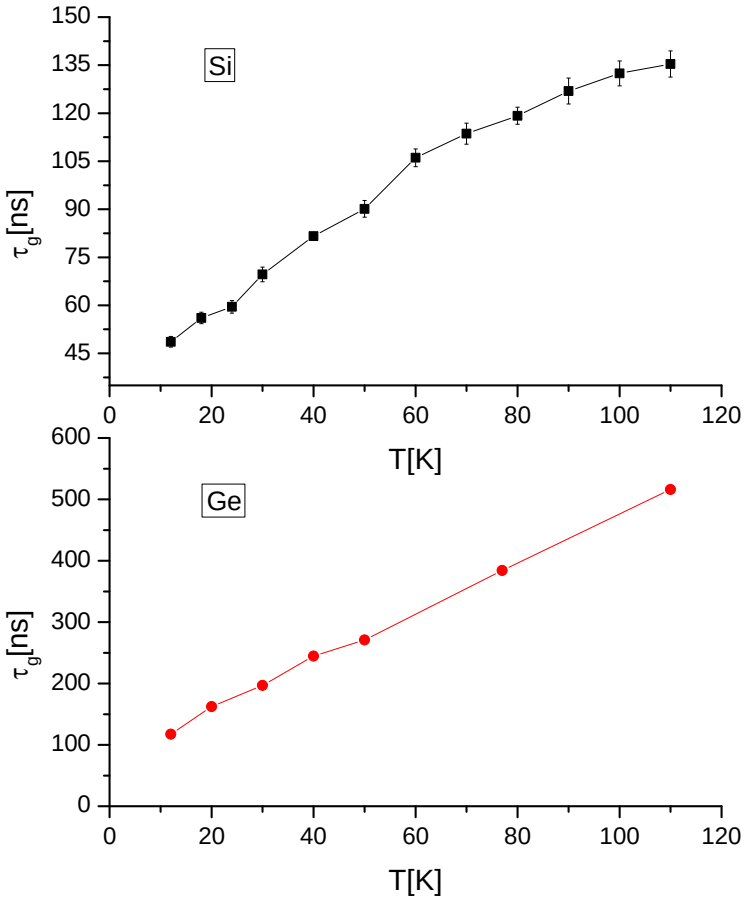

Figure 5.1.3.6. The change of dynamic interaction lifetime versus temperature

5.1.4. Compare the results with literatures

The dynamic interactions in elemental semiconductors like Si, Ge and in compound group III-V semiconductors GaAs were studied by A. F. Pasquevich and R. Vianden several decades ago. In these studies, the “aftereffects” and U. Bäverstam model were used and they are still valid in my measurements.

Some experimental results in this thesis are good agreements with those reported in their studies. Firstly, the anisotropy spectra obtained after removal of radiation damage

depend strongly on temperature [PAS87], [PAS90]. Secondly, the quadrupole frequency ν_Q and the relaxation parameter λ_r increase with 1/T for Si and Ge [PAS87], [PAS90]. Finally, the dynamic interactions in Si are much stronger than that in Ge, reflected by the relaxation parameter λ_r [PAS87], [PAS90]. However, there are some differences between my experimental results and their results. Firstly, in their study, the dynamic interaction happens in GaAs at low temperature from 20 K to 100 K although it is so weaker than that in Si and Ge [PAS90]. In my experiment, the dynamic interaction does not exist in GaAs at the same temperature range. The reason for this may be that the quality of GaAs used in this experiment was better than that used by A. F. Pasquevich and R. Vianden many years ago. Secondly, their result showed that for Si from 20 K to 80 K, λ_g remains constant and is equal zero, which means that the dynamic interaction does not vanish [PAS87]. In my case, λ_g is not equal zero and decreases with rising temperature T. Since the lifetime $\tau_g = \frac{1}{\lambda_g}$, the dynamic interactions exist longer at high temperature and will vanish after this lifetime.

5.2. Magnetic dipole interaction

The aim of this section is to measure the Larmor frequency by using PAC technique. In this experiment, the samples are mounted in external magnetic field with the magnitudes are 0.48 T and 2.1 T. For wurtzite structure samples like AlN and GaN, the anisotropy spectra in magnetic dipole interaction strongly depend on the orientations of the sample, which were studied in detail in the thesis of I.Agarwal [AGA12]. In my measurements, the samples are pure semiconductors and have cubic symmetric lattice, so the anisotropy spectra is independent of sample orientations.

In all measurements, the samples were laid on the plane containing four detectors and $\vec{B}$ is perpendicular to this plane which is shown in the Fig. 5.2.1. All samples were measured at room temperature (295 K). The fitted spectra are shown in figure 5.2.2 and 5.2.3. Because the magnetic fields have the constant magnitude and direction during the measuring time, the interaction has the constant amplitude and periodically changes with time. Therefore the spectra were fitted with the fixed damping $\delta = 0$. The experimental Larmor frequencies are shown in the table 5.2.1. The theoretical Larmor frequency can be calculated as follows

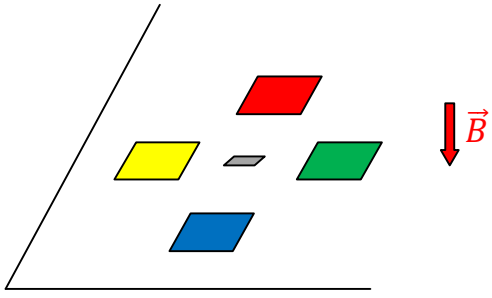

Figure 5.2.1. The orientation of samples with respect to the 4 detectors and the magnetic fields.

$$\omega_L = -\frac{g_N \mu_N}{\hbar} B_z,$$

where μ_N is the nuclear magneton, $\mu_N = 5.05\times10^{-27}$ J/T, $\hbar = 1.05 \times 10^{-34}$ Js. For ^{111}Cd, g_N = - 0.306. For the magnetic field with B = 0.48 T and B = 2.1 T, the theoretical values of Larmor frequency are 6.9 Mrad/s and 30.9 Mrad/s respectively. Comparing these values with those in the table 5.2.1, the experimental values are quite good agreement with theoretical values.

For pure semiconductor (without internal magnetic field), the Larmor frequency is proportional to the magnitude of the external magnetic field $\vec{B}$ and depends on the g- factor of the probe nucleus. The Larmor frequency is independent of the environment surrounding the probe atom.

The small differences between experimental values and the theoretical values might be due to the presence of EFG originating from the incompletely annealed samples and the systematic errors.

B[T]& T [K]	Samples	ω_{01} [Mrad/s]	ω_{02} [Mrad/s]	$\omega_{L1,2}$ [Mrad/s]	δ_1[%]	δ_2[%]	f_1[%]	f_2[%]
0.48T at RT	Ge	1.21(1)	0	6.78(3)	0	0	100	0
	Si	2.90(9)	0	6.49(2)	0	0	100	0
	InP	0.94(1)	0	7.15(5)	0	0	100	0
	GaAs	1.37(1)	0	7.49(4)	0	0	100	0
2.1T at RT	Ge	1.21(1)	0	34.09(4)	0	0	100	0
	Si	2.90(9)	0	33.55(2)	0	0	100	0
	InP	0.94(1)	0	33.47(4)	0	0	100	0
	GaAs	1.37(1)	0	33.19(7)	0	0	100	0

Table 5.2.1. The fitted parameters measured at RT in 0.48T and 2.1T for annealed samples

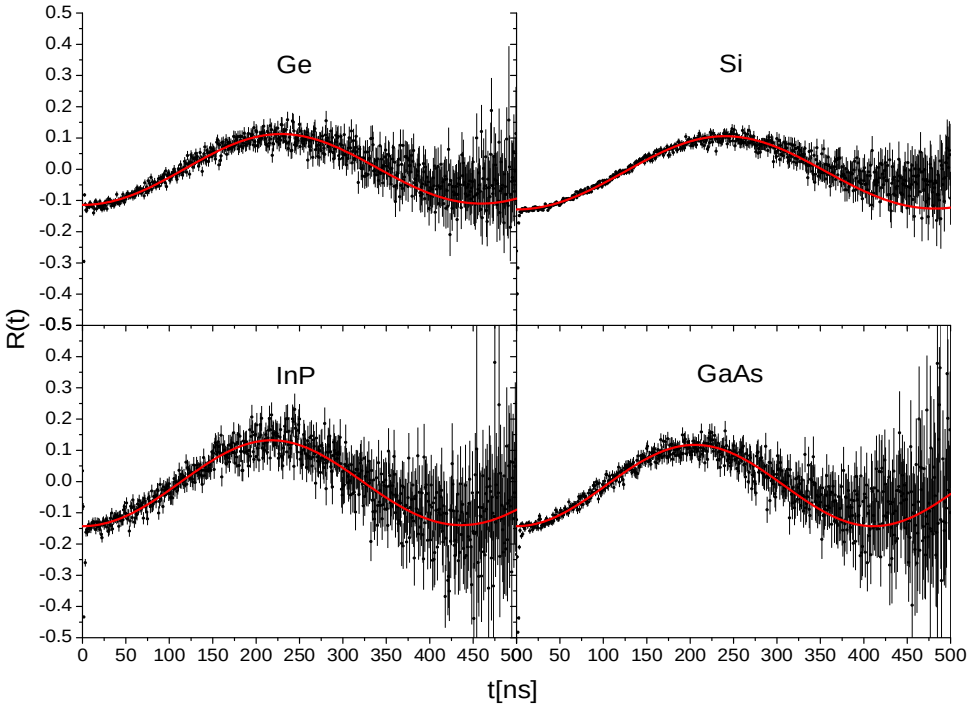

Figure 5.2.2. The fitted PAC spectra measured at RT in 0.48T for annealed samples

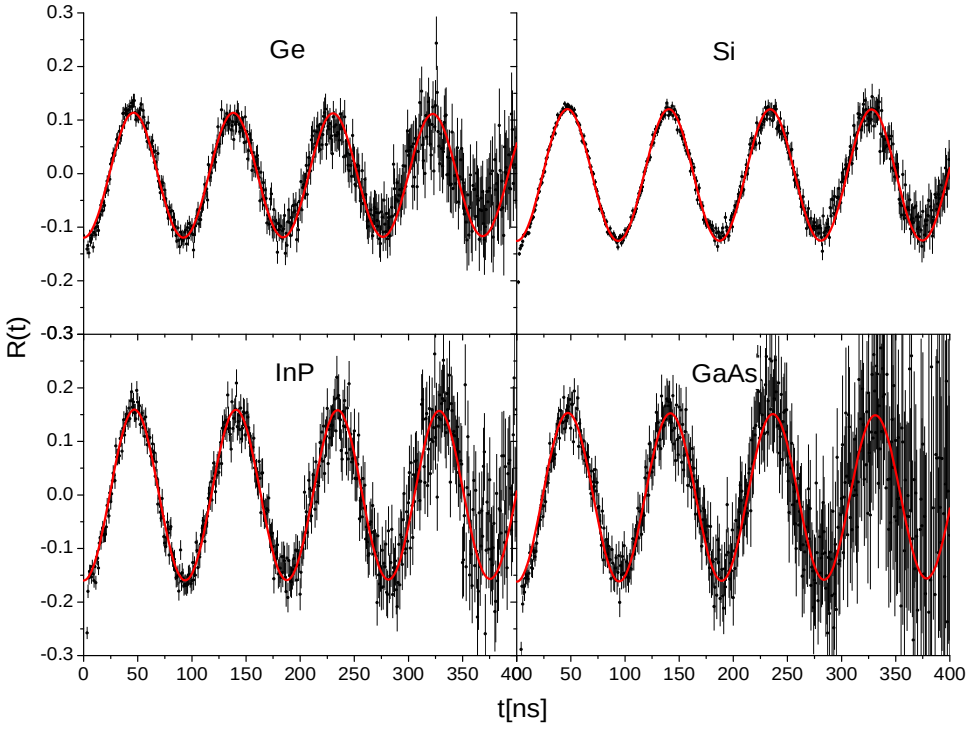

Figure 5.2.3. The fitted PAC spectra measured at RT in 2.1T for annealed samples

5.3. Combination of electric quadrupole and magnetic dipole interaction

As introduced, the main aim of this part is to show how the Larmor frequency influences on the quadrupole interaction frequency of dynamic interaction. The samples were oriented like in Fig. 5.2.1. In these measurements, the samples were mounted in the external magnetic field of 0.48 T and placed in liquid nitrogen (77 K). For Ge and Si, the interaction is supposed to be the combination of electric quadrupole and magnetic dipole interaction because besides magnetic field, there is the presence of EFG produced by "aftereffect" at low temperature. For GaAs and InP, the electric interaction is weak, as shown in section 5.1.3, and therefore only the magnetic interaction is considered. This can be illustrated by the obtained parameters in table 5.3.1 and figure 5.3.1. In fact, the spectra for InP and GaAs (Fig.5.3.1) change inconsiderably compared to those measured at RT (Fig.5.2.2). The experimental Larmor frequencies in this experiment are 6.54(6) Mrad/s and 7.08(7) Mrad/s for InP and GaAs respectively.

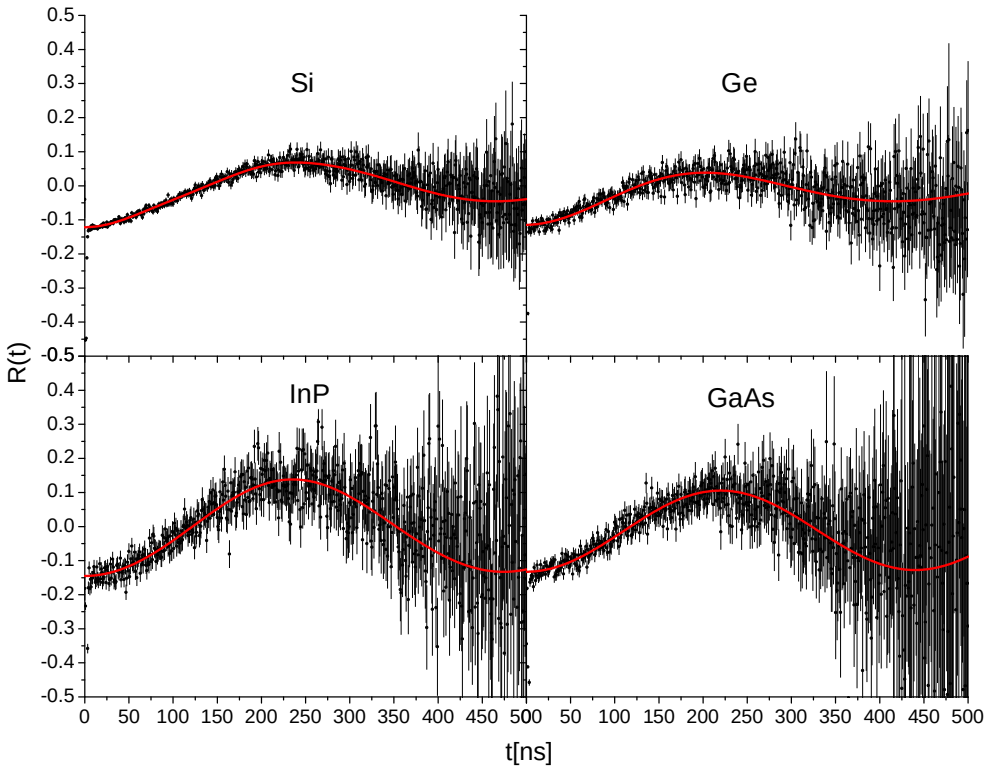

Figure 5.3.1. The fitted PAC spectra measured at 77K in 0.48T for annealed samples

For Si, the electric interaction frequency measured at 77 K without external magnetic field is $\omega_0 \approx 14$ Mrad/s (Appendix A.2), which is twice higher than theoretical Larmor frequency $\omega_L = 6.9$ Mrad/s. Therefore, the magnetic interaction is assumed to damp the electric interaction [AGA12], shown by the increasing damping 110(1) %. As a result, in this experiment, the electric frequency $\omega_0 = 10.3(4)$ Mrad/s (Fig.5.3.1) < 14 Mrad/s (Appendix A.2). Regarding Ge, the electric interaction at 77 K is so weak, $\omega_0 = 2.23(1)$ Mrad/s (Appendix A.2) that it cannot cause any influence on the magnetic interaction. Hence, the experimental Larmor frequency $\omega_L = 7.38(9)$ Mrad/s. In both samples, the damping values have been increased due to the "aftereffect", and the fractions of the probe atoms exposed into the interaction also differ from those at RT (Table 5.2.1).

B[T]& T [K]	Samples	ω_{01} [Mrad/s]	ω_{02} [Mrad/s]	$\omega_{L1,2}$ [Mrad/s]	δ_1[%]	δ_2[%]	f_1[%]	f_2[%]
0.48T at 77K	Ge	1.49(0)	0	7.38(9)	6(1)	0	90(5)	10 (1)
	Si	10.3(4)	0	6.80(4)	110(1)	0	29 (1)	71(6)
	InP	1.3(2)	0	6.54(6)	0	0	100	0
	GaAs	1.2 (2)	0	7.08(7)	0	0	100	0

Table 5.3.1. The fitted parameters measure at 77K in 0.48T for annealed samples

From these data evaluations we might conclude that when electric and magnetic interactions are combined together, in the PAC spectra, it is assumed that the weaker interaction leads to damping of the stronger. [AGA12]. For instance, if the electric interaction is dominant, the magnetic interaction will make the electric interaction weaker, which means that the quadrupole frequency ν_Q will be decreased. This shows clearly in the case of measuring at 77 K in the magnetic field of 0.48T the annealed Si.

6. Conclusion

The TDPAC technique has been successfully applied to get information about nanostructures and charge distributions in samples at atomic scale. The electric interaction between EFG and electric quadrupole moment *Q* of the probe nucleus causes the perturbation of angular correlation of two gamma rays emitted from ^{111}In decay. The evaluation of the perturbation factor *G(t)* gives us all information about the electric interactions from which we can understand more about the characteristics of the lattice structures.

The EFG originates from two possible sources: non-cubic lattice samples and the "aftereffects". After annealing to remove damage, the lattices recover their cubic symmetry, so the EFG vanishes in the cubic lattice samples. For the studied samples measured at low temperatures, ranging from 12K to 110K, the binding of holes created by the "aftereffect" to the probe nuclei leads to the fluctuating EFG. Therefore, the electric interaction is dynamic interaction at the low temperatures.

The dynamic interactions were well described by the fitted parameters such as the fractions, frequency ν_Q and damping δ, obtained from the fitted PAC spectra. According to this, the dynamic fraction f_1 decreases significantly at higher temperature T whereas the opposite is true for the static fraction f_2. The interaction frequency ν_Q is inversely proportional to temperature *T*. The damping δ rises with the temperature T. These three dependent interaction parameters together characterize for dynamic interactions. The relation among three parameters may be determined by the relaxation constant λ_r and recovery constant λ_g suggested by U. Bäverstam and R. Othaz. The U. Bäverstam and R. Othaz model has successfully described the dynamic interaction via the change of the relaxation constant λ_r and the lifetime of dynamic interaction τ_g with T, where λ_r represents the strength of the dynamic interaction and τ_g is the life time of the dynamic interactions. At the measured temperature range, λ_r decreases with rising temperature, which means that the dynamic interaction is weaker at high temperature. Moreover, the strength of dynamic interaction is different for various semiconductors. The dynamic interactions in elemental semiconductors like Ge and Si are much stronger than that in compound semiconductors like GaAs, InP. The results show that the electric interactions have not occurred in annealed GaAs, InP at all measured temperatures. Regarding to τ_g, it also increases with the temperature T, which means that the dynamic interaction exists longer at high temperature.

Further, as introduced, we are looking for the influence of the magnetic interaction on the dynamic damping. The results in section 5.3 show that this become true when we measured at 77K in the magnetic field of 0.48 T the annealed Si. The magnetic field may damp the EFG, making a larger dynamic damping.

Appendix

A. The fitted parameters

A.1 Fitted parameters measured at low temperature range for annealed Ge

T[K]	ω_{01}[Mrad/s]	ν_{Q1} [MHz]	δ_1[%]	f_1[%]	f_2[%]	λ_r[MHz]	λ_g[MHz]	τ_g[ns]
12	9.75(6)	10.34(6)	125(1)	30.1(1)	69.9(2)	3.67(6)	8.5(1)	117(2)
20	6.07(2)	6.43(2)	142(1)	28.4(1)	71.6(2)	2.44(4)	6.2(1)	162(3)
30	4.67(3)	4.95(3)	151(1)	27.8(1)	72.2(3)	1.95(4)	5.1(1)	197(4)
40	3.62(3)	3.84(3)	154(2)	26.9(1)	73.1(3)	1.50(4)	4.1(1)	245(6)
50	3.20(2)	3.39(2)	157(1)	26.5(1)	73.5(3)	1.33(2)	3.7(1)	271(5)
77	2.23(1)	2.36(1)	158(1)	26.3(1)	73.7(3)	0.93(2)	2.60(4)	384(6)
110	1.65(1)	1.75(1)	159(1)	26.1(1)	73.9(4)	0.68(1)	1.93(4)	516(10)

(ν_{Q2} = 0 and δ_2 = 0 for all temperatures)

A.2 Fitted parameters measured at low temperature range for annealed Si

T[K]	ω_{01}[Mrad/s]	ν_{Q1} [MHz]	δ_1[%]	f_1[%]	f_2[%]	λ_r[MHz]	λ_g[MHz]	τ_g[ns]
12	72.4(9)	76.7(9)	55(2)	48.5(2)	51.5(2)	19.4(9)	20.6(9)	49(2)
18	58.6(7)	62.1(7)	57(2)	46.9(2)	53.1(2)	15.7(7)	17.8(8)	56(3)
24	46.3(6)	48.9(6)	65(2)	44.1(2)	55.9(3)	13.3(6)	16.8(8)	60(3)
30	37.8(5)	40.1(5)	67(2)	43.1(2)	56.9(3)	10.9(5)	14.4(7)	70(3)
40	29.6(2)	31.4(2)	68(1)	39.1(9)	60.9(1)	7.9(3)	12.3(3)	82(2)
50	24.3(3)	25.7(3)	72(2)	36.7(2)	63.3(3)	6.4(3)	11.1(5)	90(4)
60	19.4(2)	20.5(2)	73(2)	33.5(2)	66.5(3)	4.7(2)	9.4(4)	106(4)
70	16.9(2)	17.9(2)	75(2)	30.8(2)	69.3(4)	3.9(2)	8.8(4)	114(5)
80	14.6(1)	15.4(1)	80(2)	28.5(1)	71.5(3)	3.3(1)	8.4(3)	119(4)
90	12.7(1)	13.4(1)	84(3)	25.6(2)	74.4(5)	2.7(1)	7.9(4)	127(6)
100	11.7(1)	12.4(1)	86(2)	24.6(1)	75.1(4)	2.5(1)	7.6(3)	132(6)
110	10.9(2)	11.5(2)	88(2)	23.1(1)	76.9(5)	2.2(1)	7.4(3)	135(6)

(ν_{Q2} = 0 and δ_2 = 0 for all temperatures)

A.3 Fitted parameters measured at low temperature range for annealed InP

T[K]	$\boldsymbol{\omega}_{02}$ [Mrad/s]	ν_{Q2} [MHz]	δ_2[%]	f_2[%]	λ_{2r}[MHz]	λ_g[MHz
12	0.87(2)	0.92(2)	0	100	0	0
20	0.85(1)	0.90(1)	0	100	0	0
30	0.87(1)	0.92(1)	0	100	0	0
50	0.83(2)	0.88(2)	0	100	0	0
70	0.82(2)	0.87(2)	0	100	0	0

(f_2, ν_{Q2}, δ_2 belong to the static interaction; ν_{Q1} = 0 and δ_1 = 0 for all temperatures)

A.4 Fitted parameters measured at low temperature range for annealed GaAs

T[K]	ω_{02} [Mrad/s]	ν_{Q2} [MHz]	δ_2[%]	f_2[%]	λ_{2r}[MHz]	λ_g[MHz]
12	1.25(2)	1.32(2)	0	100	0	0
20	1.13(2)	1.20(2)	0	100	0	0
30	1.05(2)	1.11(2)	0	100	0	0
40	1.03(1)	1.09(1)	0	100	0	0
50	0.95(1)	1.01(1)	0	100	0	0
60	0.93(1)	0.99(1)	0	100	0	0
70	0.86(1)	0.91(1)	0	100	0	0

(f_2, ν_{Q2}, δ_2 belong to the static interaction; $\nu_{Q1} = 0$ and $\delta_1 = 0$ for all temperatures)

A.5. Error calculations:

$$\Delta\nu_Q = \nu_Q . \frac{\Delta\omega_0}{\omega_0} = \frac{10}{3\pi}\Delta\omega_0$$

$$\Delta\lambda_r = \lambda_r \sqrt{\left(\frac{\Delta f_1}{f_1}\right)^2 + \left(\frac{\Delta\delta}{\delta}\right)^2 + \left(\frac{\Delta\omega_0}{\omega_0}\right)^2}$$

$$\Delta\lambda_g = \lambda_g \sqrt{\left(\frac{\Delta f_2}{f_2}\right)^2 + \left(\frac{\Delta\delta}{\delta}\right)^2 + \left(\frac{\Delta\omega_0}{\omega_0}\right)^2}$$

$$\Delta\tau_g = \frac{\Delta\lambda_g}{\lambda_g}\tau_g$$

B. The PAC spectra

B.1 Fitted TDPAC spectra measured at low temperature range from 12 K to 110 K for annealed Ge

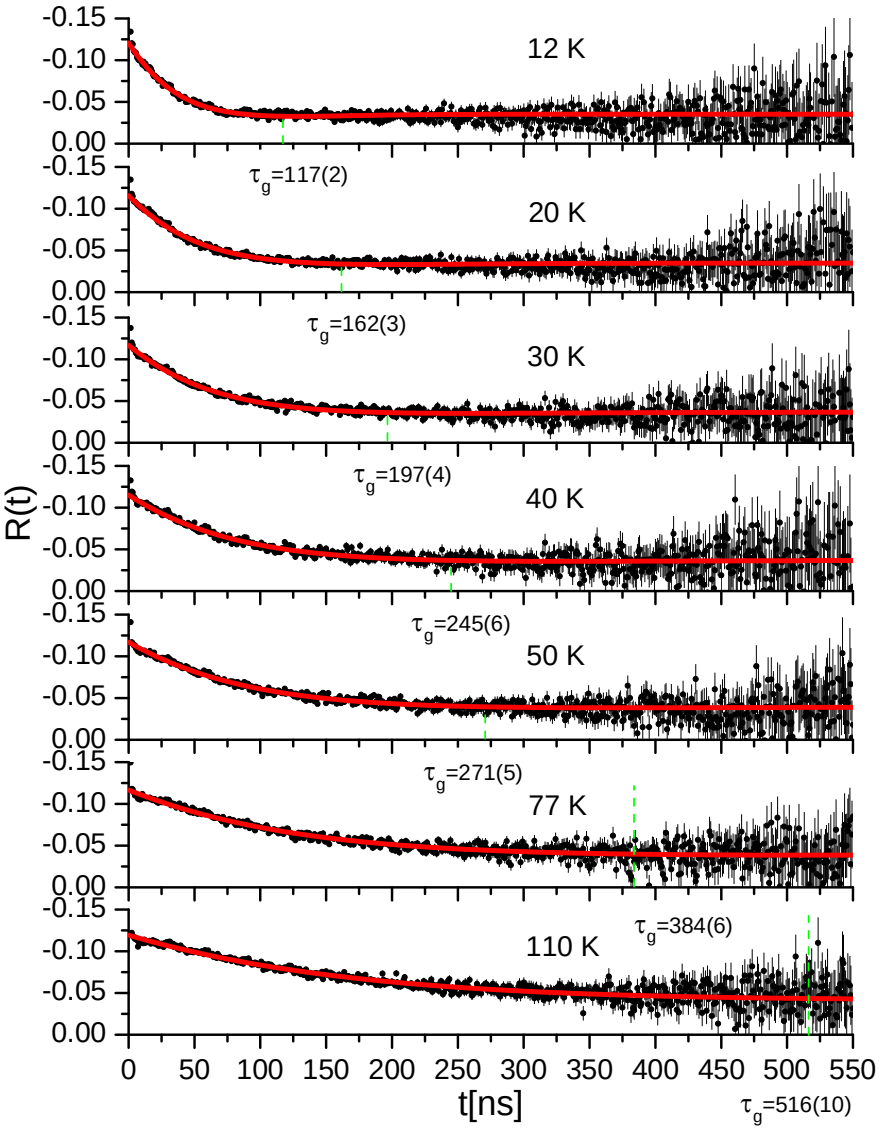

B.2 Fitted TDPAC spectra measured at low temperature range from 12 K to 110 K for annealed Si

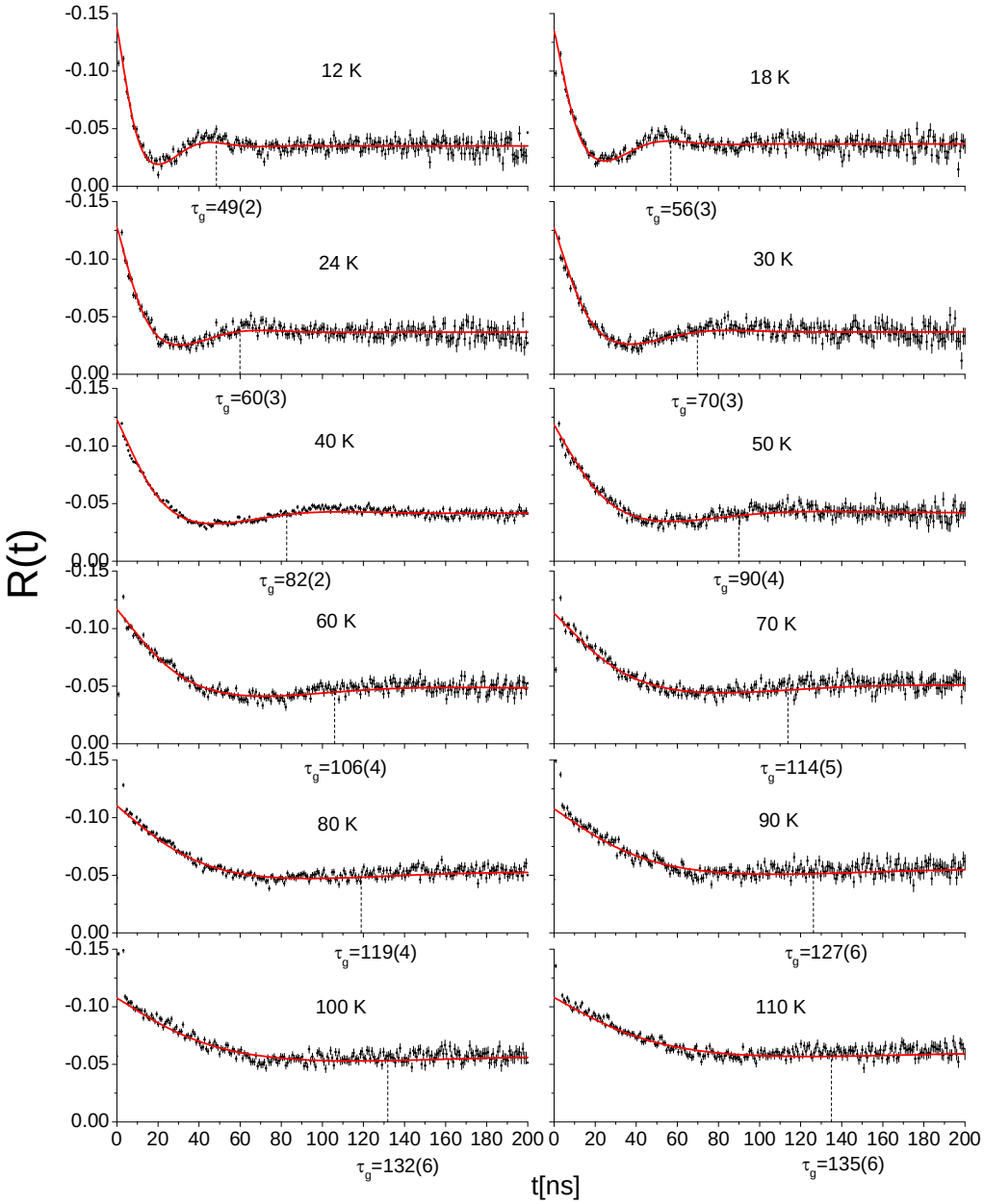

B.3 Fitted TDPAC spectra measured at low temperature range from 12 K to 70 K for annealed InP

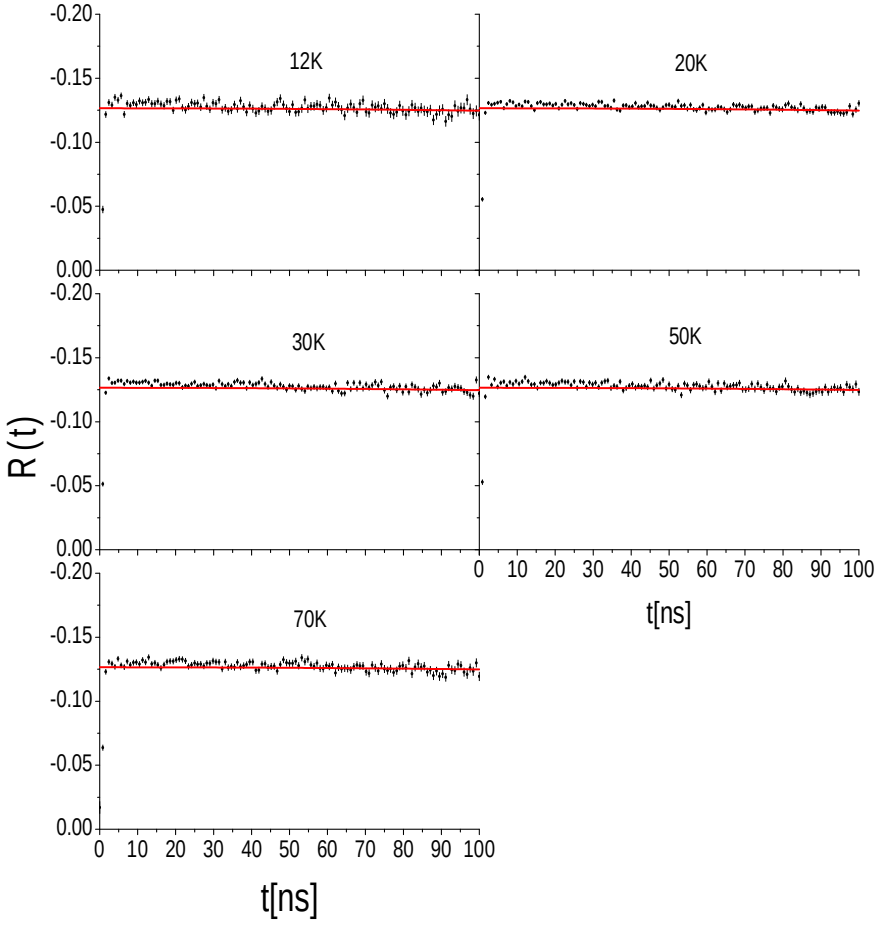

B.4 Fitted TDPAC spectra measured at low temperature range from 12 K to 70 K for annealed GaAs

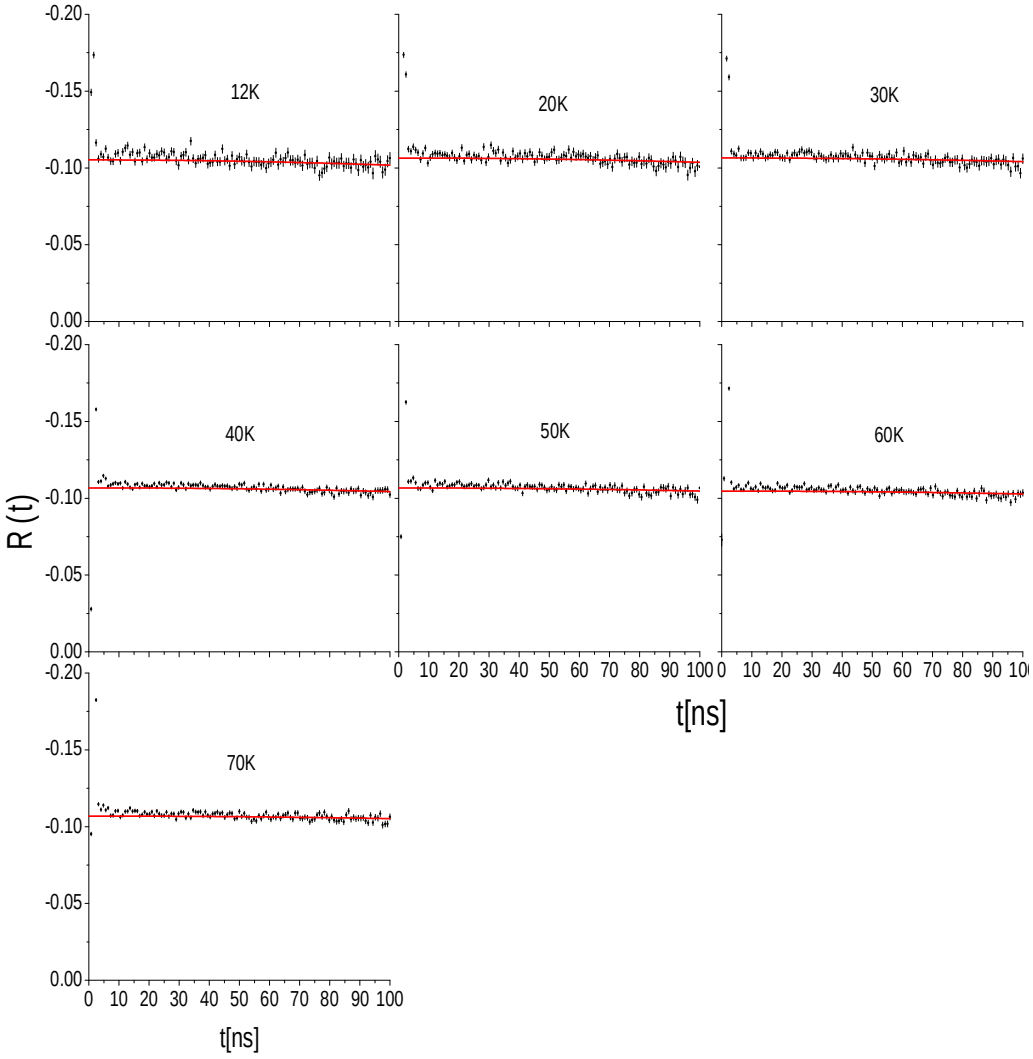

References

[ABR53] **A. Abragam and R. V. Pound**, *Influence of Electric and Magnetic Fields on Angular Correlations,* Physical Review 92, 943 (1953)

[AGA12] **I. Agarwal**, *Influence of Magnetic Fields on a Defect-Complex in Group-III Nitride Semiconductors,* Master Thesis, HISKP University of Bonn (2012)

[ARE80] **A. R. Arends, C. Hohenemser, F. Pleiter, H. de Waard, L. Chow, R.M. Suter**, *Data reduction methodology for perturbed angular correlation experiments*; Hyp. Int. 8, 191–213 (1980)

[BAR10] **A. R. Barron**, *Properties of Gallium Arsenide*, Jan 22, 2010. This work is produced by The Connexions Project and licensed under the Creative Commons Attribution License.

[BAR92] **N. P. Barradas**, *NNFIT the PAC Manual*, Lissabon, 1992.

[BÄV72] **U. Bäverstam, R. Othaz, N. de Sousa and B. Ringström**, *After-effects in the decay of ^{75}As and ^{197m}Hg,* Nuclear Physics A, Volume 186, Issue 3, Pages 500–512, 23 May 1972

[BRI91] **J.C.Brice**, *Properties of Indiumphosphide*, published by INSPEC, the Institution of Electrical Engineers, London and New York.The Institution of Electrical Engineers (1991)

[BLA82] **J. S. Blakemore**, *Semiconducting and other major properties of gallium arsenide*, J. Appl. Phys. 53(10). October 1982

[DEI93] **M. Deicher**, *Dynamics of defects in semiconductors,* Hyperfine Interactions 79, 681-700, © J.C. Baltzer AG, Science Publishers (1993)

[FRA65] **H.Frauenfelder, R.M.Steffen**; *Alpha-, Beta-, and Gamma-Ray Spectroscopy*; Vol.2, Hrsg. K. Siegbahn, Amsterdam (1965)

[HAM10] **S. Hamidi** , *Implantation studies of 111In in group-III nitride ternary semiconductors* , Master thesis, HISKP University Bonn, November 10, 2010.

[HEM04] **L. Hemmingsen, K. N. Sas, E. Danielsen**, Biological Applications of Perturbed Angular Correlations of γ-Ray Spectroscopy, Chem. Rev.104,4027−4061 (2004)

[MEY70] **J.W.Meyer, L.Eriksson, and J.A.Davies**, *Ion Implantation in Semiconductors* (Academic, New York, 1970)

[MOL03] **G. T. Mola**, *Indium-impurity pairs in semiconductors and the study of the influence of uniaxial stress on defect complexes in silicon*, Ph.D thesis, HISKP University of Bonn (2003)

[NÉD07] **R. Nédélec**, *Seltene Erden in GaN und ZnO untersucht mit der PAC-Methode*, PhD thesis, Rheinischen Friedrich -Wilhelms - Universität Bonn, 2007.

[PAS87] **A. F. Pasquevich and R. Vianden,** *Temperature dependence of the hyperfine interactions of ^{111}Cd in silicon*, Physical Review B Volume 35, Number 4, 1560, February 1987.

[PAS88] **A. F. Pasquevich and R. Vianden,** *Temperature dependence of the hyperfine interactions of ^{111}Cd in germanium*, Physical Review B Volume 37, Number 18, 10858, June 1988.

[PAS90] **A. F. Pasquevich and R. Vianden,** *Time-differential perturbed-angular-correlation study of ^{111}In-^{111}Cd in III-V compounds*, Physical Review B Volume 41, Number 16, 10956, June 1990.

[PFE92] **W.Pfeiffer, M.Deicher, R.Kalish, R. Keller, R. Magerle, N. Moriya, P. Pross, H. Skudlik, Th. Wichert, H. Wolf and ISOLDE Collaboration**, *Annealing of Damage in GaAs and InP after Implantation of Cd and In*, Materials Science Forum Vols. 83-87 (1992) pp 1481-1486 © (1992) Trans Tech Publications, Switzerland

[PIC04] **P.Pichler**, Intrinsic point defects, impurities, and their diffusion in silicon, Springer – Verlag/Wien, 2004.

[RIS00] **M. Risse**, *Das Verhalten von Brom in InAs und GaAs, untersucht mit den Sonden ^{77}Br(^{77}Se), ^{79}Br und ^{82}Br*, PhD thesis, HISKP Uni Bonn, 2000

[SAN09] **N. Santen**, *Dotierungsabhängigkeit des elastischen Verhaltens von Silizium*, PhD thesis, HISKP Uni Bonn, 2009

[SCH84] **F. Schneider, S. Unterricker**, *Radiation Damage and Its Annealing Behaviour in InP after Recoil Implantation of ^{118}Sb and ^{111}In Observed by TDPAC*, phys. stat. sol. (a) 85, 455 (1984)

[SCH92] **G. Schatz, A. Weidinger**, Nuclear Condensed Matter Physics, John Wiley and Son, New York (1992)

[SHA05] **J. F. Shackelford**, *Introduction to materials Science for Engineers*, Pearson Education, Inc., Upper Saddle River, NJ (2005)

[SHP02] **L. G. Shpinkova, A. W. Carbonari, S. M. Nikitin, J. Mestnik-Filho**, *Influence of electron capture after-effects on the stability of $^{111}In(^{111}Cd)$-complexes with organic ligands*, Chemical Physics 279:255-263, Chemical Physics 279, 255–263 (2002)

[SIM11] **R. E. Simon**, *Implantation studies on silicon doped group-III nitride semiconductors*, Master thesis, HISKP University of Bonn, 2011

[SLA64] **J. C. Slater**, *Atomic Radii in Crystals*, J. Chem. Phys. 41, 3199 (1964)

[STE10] **M. Steffens, J. Penner, H. Kamleh, R. Vianden**, *Temperature dependence of the hyperfine fields of ^{111}In in sapphire (Al_2O_3) single crystal*, © Springer Science+Business Media B.V. (2010)

[SZE81] **S. M. Sze**, *Physics of Semiconductor Devices, John Wiley & Sons (1981)*

[TEC78] Technical Manual for Displex Closed-Cycle Refrigeration System Models CSA-202, CSW-202 and HV-202, Manufactured by Air products and Chemicals, Inc, 1978

[THU70] **J. E. Thun**, *Proc. Int. Conf. on angular correlations in nuclear disintegrations*, Delft, August 17-21, 1970

Acknowledgments

First of all, I would like to express my gratitude to Priv. Doz. Dr. Reiner Vianden for his excellent supervision. He was always present to answer my questions and to help me to solve technical problems in the laboratory, and so much more. Without his supports I cannot finish my thesis.

I would also like to express my gratitude to Prof. Dr. Karl Maier who agreed to be the second examiner.

I would like to thank the Isotope Separator group for their very kind helps in the Indium implantations.

Further, I would also like to extend my thanks to all the members in our research group, who always help me to solve any problems when I needed. The nice time we had together will be unforgettable in my life. I specially thank Juliana for all her helps in using Nightmare program and many other things. I really thank Michael for his kind help in the data analysis and in correcting my thesis.

Finally, I am very thankful to the Mekong and DAAD scholarships for their financial supports. Without these supports I could not follow this Master program.